Delft University of Technology

Bachelor of Science Thesis
Faculty of Applied Sciences

Flow-influenced electrical conduction in a Semi-Solid Flow Battery

Author:
Hugo Korthals Altes (4384601)

Supervisor and examiner:
Martin Rohde

2^{nd} *examiner:*
Erik Kelder

February 10, 2020

Abstract

In this report the electrical conduction of the Semi-Solid Flow Battery is analyzed and described as a function of multiple factors. The research goal of the project is to analyze the electrical conduction of the fluid that separates the active materials from the electrodes. Since the Semi-Solid Flow Battery (SSFB) relies on the principle of a flowing fluid in which the active material is dispersed, this report focuses on the effect of the fluid flow profile on the electrical conduction. The electrical conduction has been analyzed using two methods. These methods connect the known theoretical background to the specific characteristics of the flow cell, in which the energy is exchanged. The first method in this report consists of a simulation relying on the principle of the percolation theory. By dividing a system into small cubes that can either contain electrical conducting material or represent electrical insulating material, the effect of changes in the volume fraction of electrical conducting material on the possibility of the exchange of electrons between the active material and the electrodes is investigated. The results extend the knowledge of the percolation theory to the possibility of electron exchange between a single point (the active material) and a plate (the electrode). As long as a system representing a fluid consists of a realistic number of particles, the distance between the active material and the electrode does not affect the possibility of electrical conduction.

In the second method, by extracting data from rheo-electrical experiments with a fluid consisting of aqueous carbon black particles, a relation between the average velocity and the electrical conduction is obtained. This relation is obtained in a Poiseuille flow between two plates with dimensions significantly larger than the distance between the plates. After defining the characteristics of the flow cell, a clear peak can be observed in the average resistivity for a certain average velocity, depending on the height of the flow. This peak marks the velocity at which the average conductivity is lowest and therefore denotes the situation to be avoided to assemble a flow cell that allows for optimal energy transition. To reduce uncertainty, the obtained relation requires a larger dataset to fit a curve to, therefore repetition of the rheo-electrical experiments can be useful for more accurate and insightful results.

This report is part of the Bachelor thesis of Applied Physics at the University of Technology in Delft.

Contents

1 Introduction

1.1 Energy demand

In a world where energy consumption is continuously increasing (see figure 1) and the awareness of climate change forces us to minimize carbon dioxide emission, we more and more rely on renewable energy sources. Usage of solar and wind energy, provided by the sun and the differences in atmospheric pressure, is one of the ways to a carbon-neutral energy consumption. However, while the use of these energy sources is increasing, their availability is not as reliable as the availability of energy sources like fossil fuels. Without the use of an energy storage or energy transportation method, solar energy for example is only available when the sunlight reaches the surface of a solar panel. Therefore it is not available at night, when energy demand is still present. On top of that, the power of these energy sources may vary per season (see figure 2), depending on the local climate. To overcome these daily or seasonal fluctuations, surplus energy that is produced when the local energy demand is lower than the supply, needs to be stored stationary for later use or transported to areas with an energy shortage.

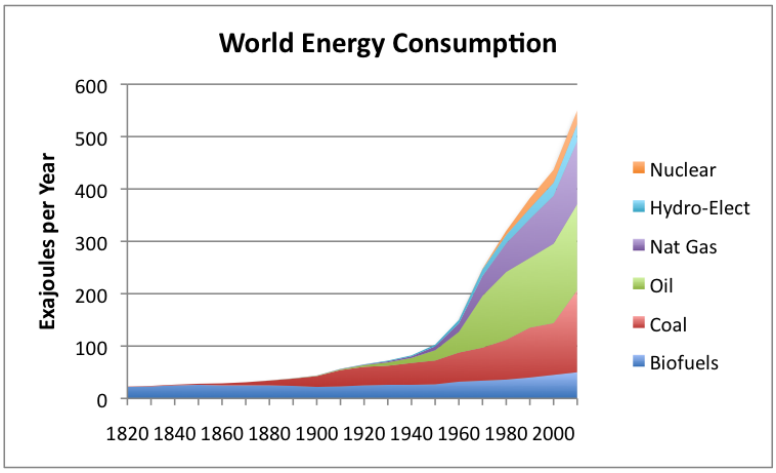

Figure 1: The increase of energy consumption over the years per source. Based on Vaclav Smil estimates together with BP Statistical Data for 1965 and subsequent[12].

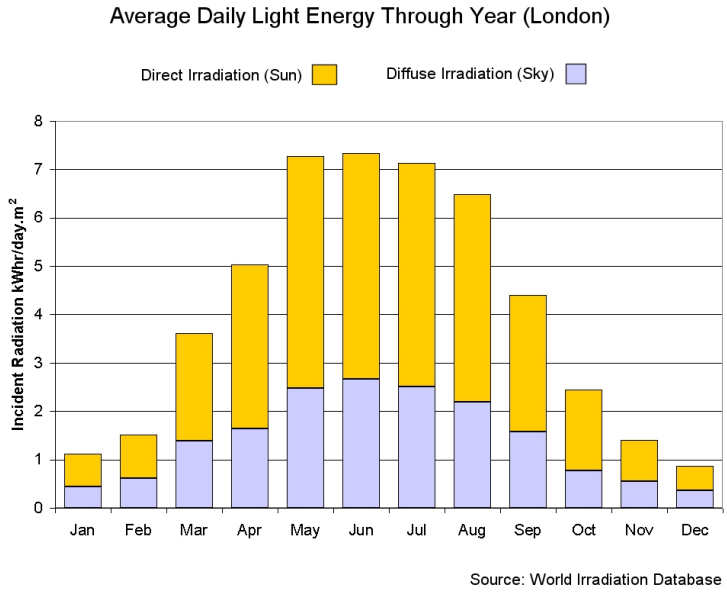

Figure 2: Seasonal fluctuations of solar energy in London [13]

1.2 Energy storage

When storing energy for later use or for transport to another part of the world, ideally no energy should be lost. Secondly the charge and discharge rates should be high enough to meet power demand and supply, whereas the materials should have a high density of stored energy. On top of that, the cost and durability of used materials have to meet economical and environmental demands. Because of this, the criteria to determine the usefulness of for example a battery are the power of (dis)charging, the energy loss during (dis)charging or during storage time, the capacity per volume or weight and the durability, availability or eco-friendliness of the materials in the battery.

Some types of energy storage can be efficiently integrated in the local environment, like a dam in the mountains, whereas other types are promising due to their high energy densities and charge-discharge efficiencies, like lithium-ion batteries.

1.3 Redox Flow Batteries

Lithium-ion batteries are types of batteries that store energy in so-called electrochemical materials. By changing the electrochemical structure of molecules, electrons are released or accepted and a voltage can be created between two types of materials. These reactions, where electrons are transferred between different molecules or atoms, are called reduction-oxidation (Redox) reactions. The electrochemical materials can be stored and used in different states of matter, like solid or aqueous, with different energy densities, power capacities and efficiencies. One of the applications of electrochemical energy storage is called the Redox Flow Battery, or RFB, in which the active materials are dispersed in a fluid that circulates through reservoirs and a flow cell.

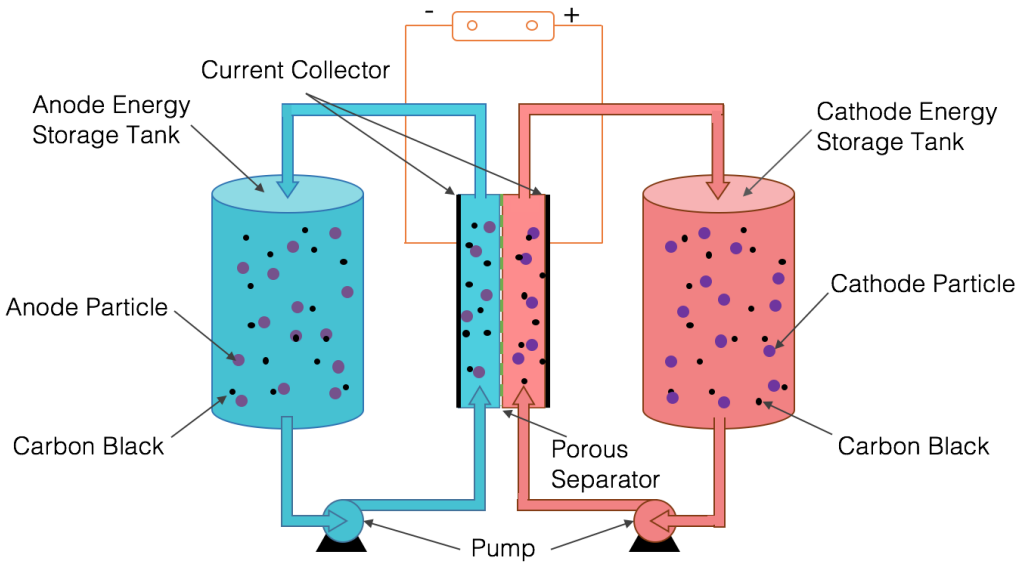

Figure 3: Schematic representation of a Redox Flow Battery

The Redox reactions take place in the flow cell (the centre of figure 3), which is designed to optimize the energy transmission from the current collectors (left and right side of the flow cell) to the active materials and vice versa. Depending on the direction of the electron flow, reduction and oxidation reactions each occur in one half of the flow cell. The reductor donates electrons (oxidation) and the oxidator accepts electrons (reduction). When the active materials discharge or charge, the electric current between the flow cell halves decreases or increases, respectively. To maintain the electric current in the circuit, and thus the power capacity of the battery, the active materials in the flow cell have to be replaced continuously. In a RFB their replacement is accomplished through a constant circulation of the liquid between the flow cell and large reservoirs. This circulation is often caused by a pump which creates a pressure difference, resulting in a constant flow through the flow cell. The energy density in these reservoirs is equal to the energy density in the flow cell. Therefore, due to the variable size of the reservoirs, RFBs can store any desired amount of total energy, while keeping the flow cell the same.

For energy to be transferred between the current collectors and the active components in the flow cell, an electrically conducting network is required that connects the active material with the current collectors. Often in RFBs, the electrode consists of a solid, porous carbon network[15][9]. This network is designed to maximize

the fraction of active material that reaches the surface area of the electrodes. The downside of this maximization is the high energy loss due to friction in the flow cell, causing the need for a higher pressure difference created by the pump.

1.4 Semi-Solid Flow Batteries

In a Semi-Solid Flow Battery, the fluid consists not only of the active material and an electrolyte; aqueous carbon black is dispersed in the liquid as well[2][10]. These electrical conducting particles form a percolating network (see figure 4) that connects active material with the current collector, functioning as an aqueous, deformable electrode that flows through the cell. This electrode allows the active materials inside the flow cell to charge or discharge without reaching the surface of the current collector. The addition of these particles reduces the need of the porous electrode in the flow cell.

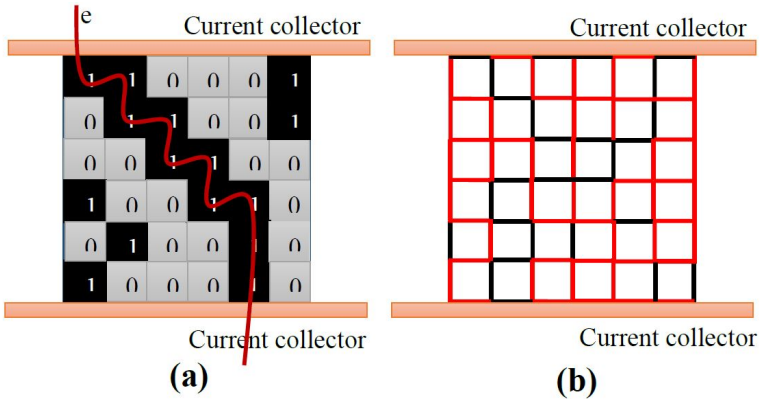

Figure 4: Site percolation (a) and bond percolation (b) in a square lattice between two current collectors[4]

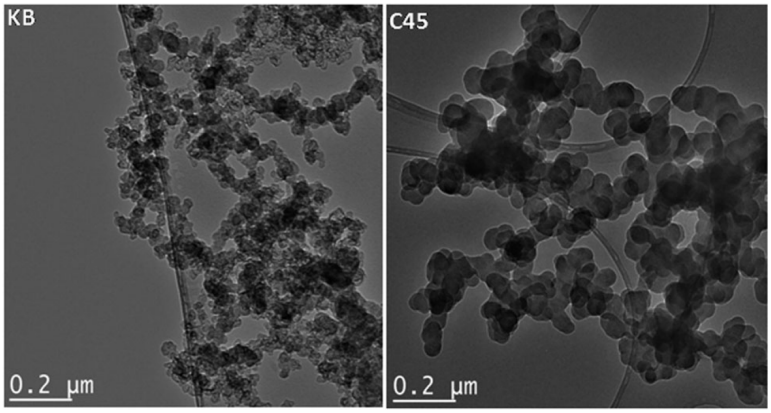

Figure 5: TEM micrographs of two carbon black types: Ketjen black EC- 300 (KB) and C-NERGYt Super C45 (C45)[16]

1.5 Problem description

Section 1.2 introduces the criteria for promising batteries. The the total energy capacity of the battery is primarily decided through the size of the reservoirs. The durability and cost of the used materials of the SSFB relies mostly on the preparation of the ion-specific membrane and the integration of the pump. However, energy efficiency and power supply are determined by the electrical conduction, and the interaction with the ionic diffusion and the friction between the fluid and the walls. To design a flow cell and choose the optimal fluid composition, an insight in the different parameters that determine electrical conduction in the flow cell is desired. From literature, it is known that the fluid in the Semi-Solid Flow Battery needs to flow through the cell to maintain the electric current in the circuit[2][10]. In other research, measurements of the rheo-electrical properties of a certain fluid containing carbon black have been performed[16]. The results of these measurements provide a relation between the rheology and the electrical conducting properties of this specific

fluid composition. However, these results have not yet been applied to the flow profiles in for example the flow cell of a Semi-Solid Flow Battery.

1.6 Research question

As introduced in section 1.5, this report describes a project on the influence different factors have on the electrical conduction in a flow cell. The effect of changes in flow cell dimensions and the effect of changes in the concentration and distribution of carbon black (CB) and the active materials are investigated while also researching the role of the flow profile. The research question therefore is:

> How does the electrical conduction relate to the height and width of the flow cell, the carbon black concentration in the fluid and the flow profile of the fluid?

2 Theoretical background

In this chapter the theoretical background of the subject of this report will be discussed. The fundamental principles of the Semi-Solid Flow Battery will be described. Section 2.1 elaborates the need for insight in the electrical conduction in the flow cell. In section 2.2 the possibility of electrical conduction is explained with the percolation theory. Section 2.3 describes a characteristic of the fluid in the flow cell and elaborates the influence of the flow profile of the fluid on the electrical conduction in the flow cell, caused by this specific characteristic.

2.1 Voltage and electric current in the battery

It's often useful to know the voltage and electric current in the circuit between the current collectors of a battery (see figure 6), during both charging and discharging. When discharging, the energy consuming end optimally performs when a constant and well-known voltage is delivered to the circuit and the electric current through the circuit is constant as well. Whether it's a single device or for example an entire city, energy optimization is often acquired when the voltage and current are as constant as possible. When charging, the same principle holds, as the energy producer or supplier often provides steady voltage and current.

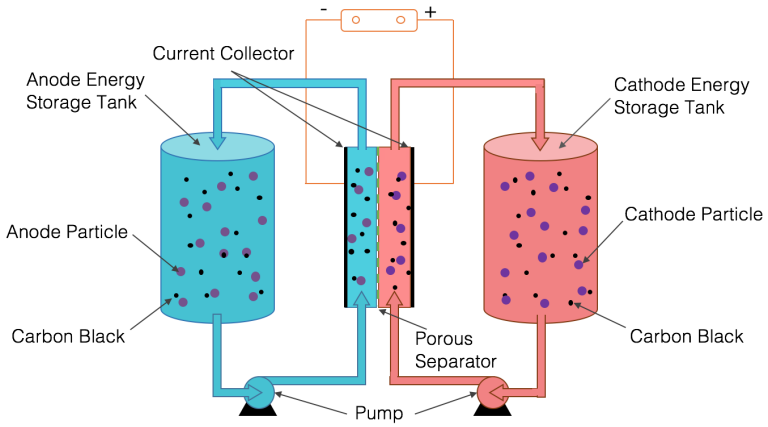

Figure 6: Schematic representation of a Redox Flow Battery. The blue and red areas mark the fluid of the Redox Flow Battery, which separates the active material from the current collector and carries the active material. The thin lines represent the circuit and the external energy source or consumer.

Because of this, it's useful to know how much voltage is applied on the circuit between the current collectors of the SSFB and what the electric current through the circuit is. For a battery to be promising, it is essential to make sure the voltage and current are as constant and as high as possible.

2.1.1 Total voltage and electric current

The total voltage between the active materials depends on the Redox potential of the active materials used at both sides of the flow cell. This means that the potential between the active materials is constant, independent of the amount of active material or the resistance of the circuit. The total electric current can be calculated by dividing the total voltage by the total electrical resistance between the active materials.

2.1.2 Voltage and electric current between the current collectors

Assuming the path between two active materials can be seen as a closed circuit, the Redox potential is distributed proportionally over the different resistances that are placed in series. As stated in equation 1, the voltage across resistor i is proportional to its resistance R_i and the total voltage potential V (in Volt), divided by the total resistance.

$$V_i = I_i * R_i = I_{tot} * R_i = \frac{V_{tot}}{R_{tot}} * R_i = \frac{V_{tot}}{R_{circuit} + R_{fluid}} * R_i \tag{1}$$

In case of a circuit with resistors placed in series only, the current through the resistor I_i equals the total current in the circuit. This means the current through the circuit between the current collectors is equal to the total electric current between the active materials. Assuming the resistance between the current collectors

$R_{circuit}$ is known and constant, the only thing left to investigate is the electrical resistance of the fluid R_{fluid} between the active material and the current collector in both flow cell halves.

2.2 The possibility of electrical conduction

As described in section 1.4, the electrical conduction in the flow cell is provided primarily by the aqueous carbon black. For the possibility of electrical conduction between the active material and the current collector, the carbon black (CB) particles in the flow cell have to form a conducting bridge from the active material to the current collector. The distance between two CB particles determines the electrical resistance between them. The closer two carbon particles are together, the lower the electrical resistance of the medium between them. If the distance between two particles is zero, they can easily exchange electrons. In figure 7, this exchange is shown in an 2D lattice with particles filling the space of a square. As seen in figure 7b, electrons can easily jump to neighbouring particles. When these particles form a connection between two different voltage potentials, electrons move in the direction of the higher voltage.

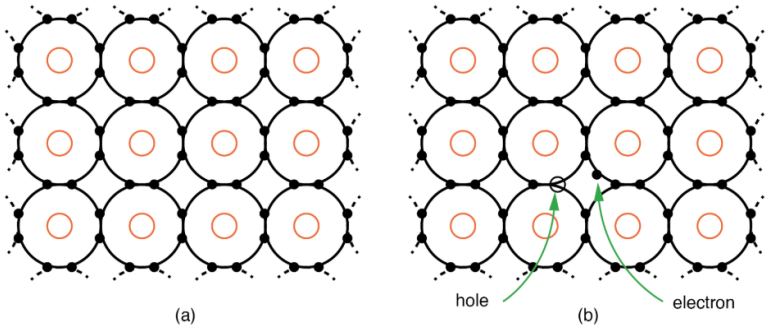

Figure 7: (a) An organised structure of conducting particles, representing the fluid when a carbon black particle (red circles) is assumed to occupy a cubical volume space. The electron shells (black circles) of two neighbouring particles overlap, therefore electrons (black dots) can be easily transferred. (b) An electron has been transferred between the electron shells of two neighbouring carbon black particles

2.2.1 The percolation theory

In figure 7, electrons can freely travel in all directions because all particles in the structure conduct electrons. However, in the fluid of the Semi-Solid Flow Battery, only a certain volume fraction contains the electrical conducting carbon black particles and electrons have to find a way from one electrode to the other, crossing only neighbouring CB particles. In figure 8, such a connection between two electrodes is shown. Every volume space has the same probability p of containing a conducting CB particle. This probability is equal to ϕ_{CB}, the volume fraction of CB particles. In the approach of the percolation theory, the remaining volume space is filled with electrically insulating material, in which electrons are insulated and therefore can not move. Whether or not two electrodes are electrically connected thus depends on the placement of conducting particles and the electrodes. According to the percolation theory, the probability of a bridge between two points depends on the fraction of conducting particles. Above a certain fraction ϕ_{CB}, called the *percolation threshold*, large clusters of conducting elements can be formed, while below this threshold the probability of cluster formation is very small[6][4].

2.2.2 Plate-to-plate distance

Gallier et al. [1] describe that the probability of two plates being connected through percolation depends not only on the volume fraction ϕ_{CB}, but also on the distance between the plates. Figure 8 is a representation of the system in which the electrical conduction is simulated by observing whether or not a percolating network can be formed between two plates. As seen in figure 9, a larger distance implies a higher percolation threshold. The threshold in this case is denoted as the volume fraction where the spanning probability $\langle \Pi \rangle$ (figure 9a) and the spanning strength $\langle P \rangle$ (figure 9b) show the most significant increase. The spanning probability is the probability that the two plates are connected by a percolating network of conducting elements. The spanning strength is the volume fraction of the medium that is connected to the plates.

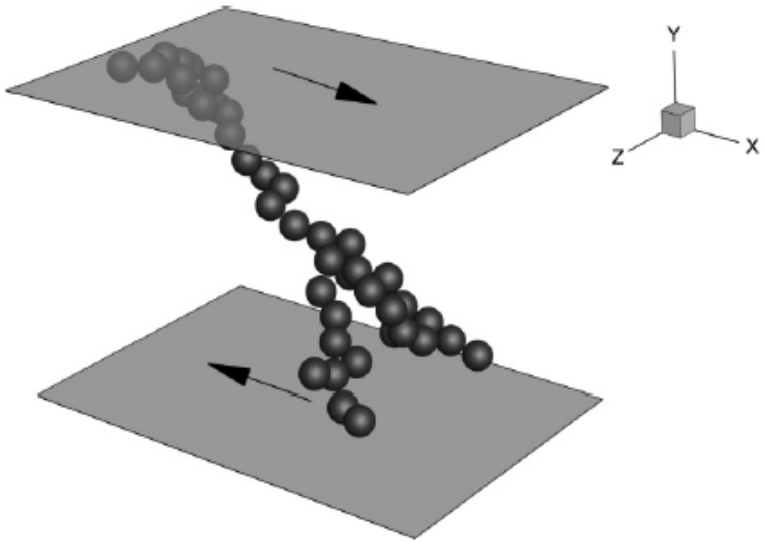

Figure 8: Visual representation of a percolating network between two plates in the simulations of Gallier et al.[1]

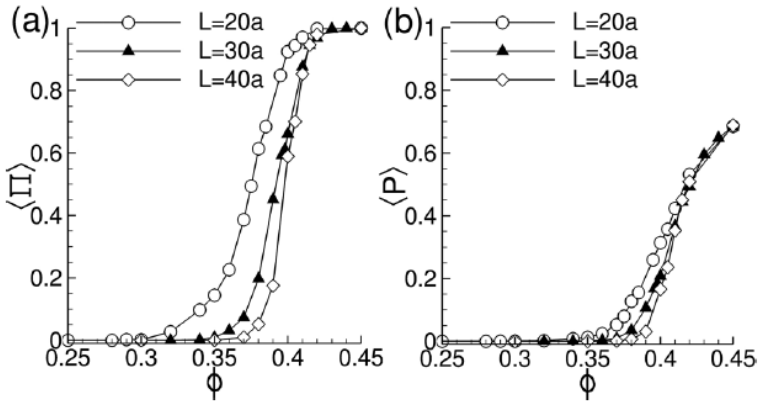

Figure 9: (a) Spanning probability $\langle \Pi \rangle$ and (b) spanning strength $\langle P \rangle$ as a function of volume fraction of electrical conducting particles ϕ for systems with different heights. The height L is denoted as the height of a number of spheres (see figure 8) with diameter a that separate the two plates.[1]

In figure 9a we see that the percolation threshold slightly varies for different heights. This means the spanning probability is lower for systems with increasing height L. The relation between the percolation theory and electrical conduction inside a fluid in general is not clear. However, percolation theory introduces a relation between the possibility of electrical conduction in a fluid and the electrode distance and carbon concentration. Note that in this approach, begin the assumption of having spherical, loose particles, the velocity of the fluid does not have any effect on the electrical conduction since the concentration of CB particles is constant.

2.3 Flow-induced electrical conduction

According to models by for example Gallier et al. [1], electrical conduction only depends on the current relative position of electrical conduction particles. The relative velocity of particles therefore seems to have no direct effect on the electrical conduction of the system. In flow cells however, this dependence exists. In this paragraph the characteristics of the carbon black particles that contribute to a flow-induced electrical conduction will be discussed. First, the characteristics that apply to the particular combination of used materials will be described. After this, the effect of these particular characteristics on the electrical conduction will be explained.

2.3.1 Agglomeration of CB particles

In suspensions consisting of particles with comparable characteristics, the different particles are distributed uniformly in space. However, carbon black particles and active material particles differ somewhat in size. Whereas the size of an individual carbon black particle is only 50 nanometer, the active material consists of particles that are often in the order of tens of micrometers in size. This causes the battery slurry to fall into a regime that is affected by colloidal forces. Van der Waals attraction between the small carbon black particles plays a huge part in the interparticle interactions of carbon black. This force causes these particles to form small agglomerations that require external forces to break[7]. Figure 10a shows two carbon black particles with radius a and interparticle distance h and a polymer brush length with thickness L. "This polymer (PVDF) is added to bind the active material with the carbon black particles and adhere them onto the current collector", according to Ma et al.[7] In figure 10b the interparticle interaction between two CB particles is shown for different particle separation distances. This interparticle potential clearly is strongest when two particles are only 2 "brush lengths" away from each other.

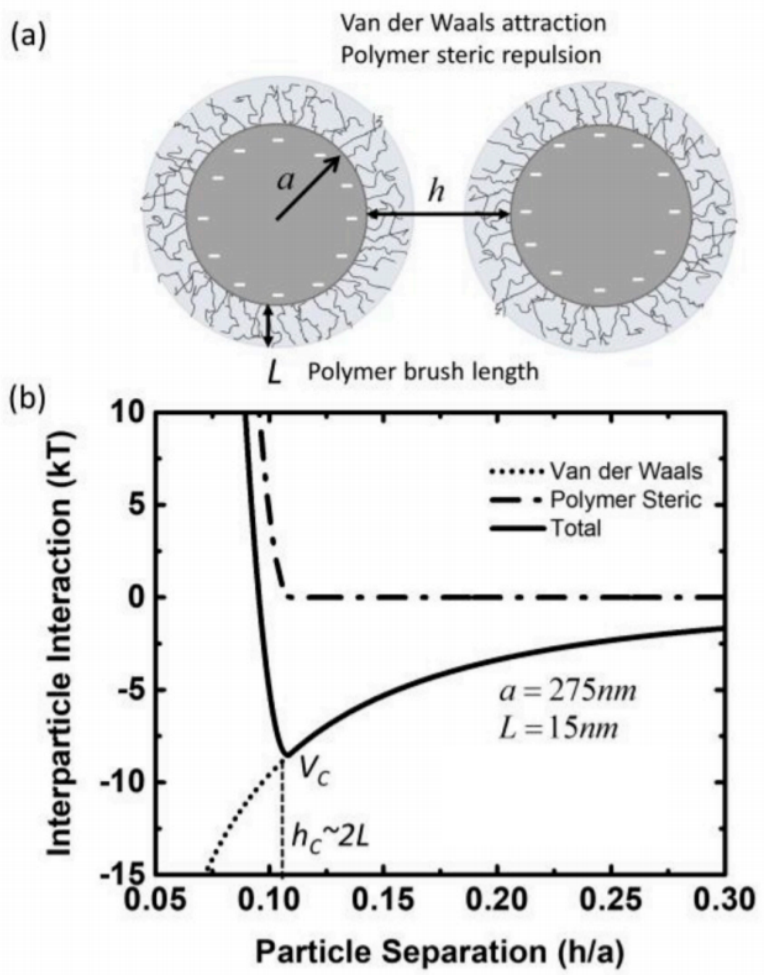

Figure 10: (a) schematic representation of two carbon black particles with radius a at relative distance h, coated in a polymer with brush length L (b) Interparticle potential between two carbon black particles[7]. $kT = k_B * T$ is equal to $4.11 * 10^{-21}$ Joule.

2.3.2 Rheology in the SSFB

When a pressure difference is applied between the two open sides of the flow cell, the fluid starts moving in the opposite direction of the pressure gradient. Friction with the walls of the flow cell causes an internal *shear stress* in the fluid. This shear stress τ depends on the relative velocity between two neighbouring compartments of the cross-section of the flow, the shear rate. As the shear rate changes, so does the shear force τ [Pa] with relation: [14]

$$\tau_{xy} = -\mu_{app} * \frac{dv_y}{dx} \tag{2}$$

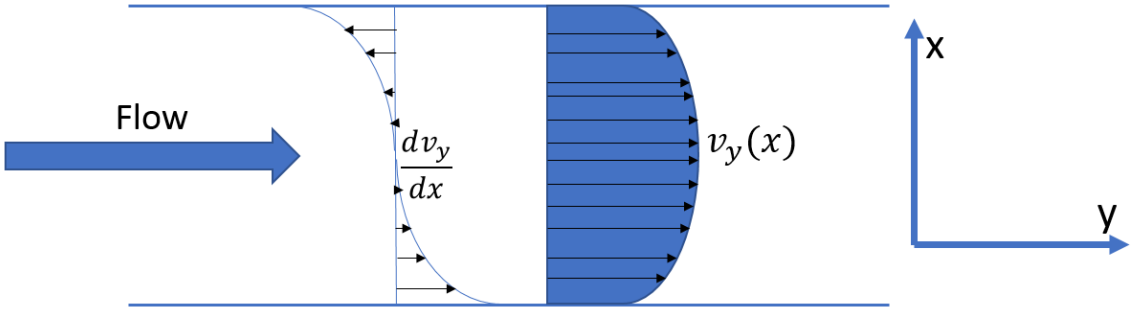

Figure 11: Profiles of the gradient of the velocity $\frac{dv_y}{dx}$ and of the velocity v_y

Here $\frac{dv_y}{dx}[s^{-1}]$, the shear rate, denotes the gradient of the velocity v_y in the direction x, perpendicular to the plane of the plates. y is the direction of the fluid flow (see figure 11). $\mu_{app}[Pa * s]$ denotes the apparent viscosity of the fluid and has to be measured for corresponding shear rate to obtain a value for the shear stress. An increase of the shear stress denotes a higher shear rate and, since the velocity of the flow at the walls is fixed and zero, denotes an increase in the average velocity of the fluid. When the shear stress is high enough, it is the external force that causes the agglomerations to break into smaller agglomerations. Figure 12 shows a relation between the shear rate in the fluid and the relative volume fraction of the carbon black agglomerations. According to a model presented by Ma et al.[7], at high shear rates the carbon black agglomerations decrease in size. This occurs for different values for the volume fraction of base particles ϕ_p.

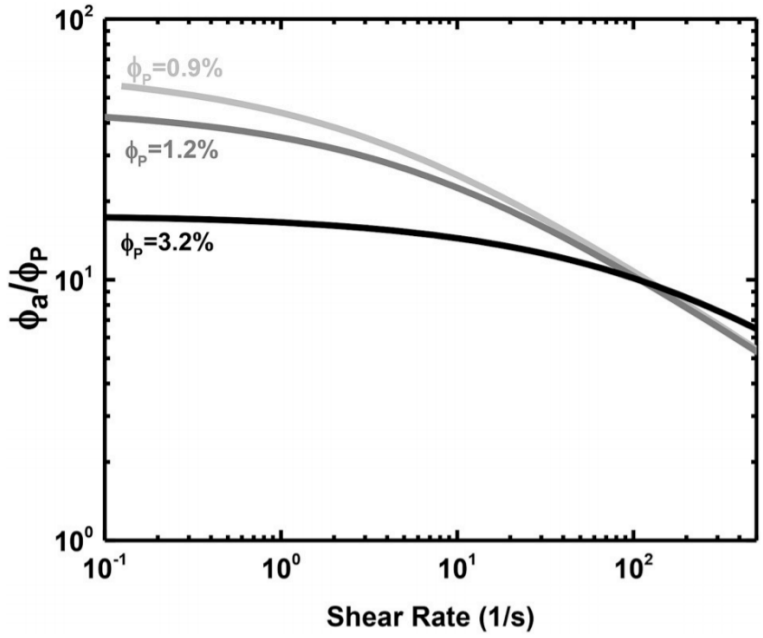

Figure 12: The relative volume fraction of agglomerations ϕ_a decreases as the shear rate increases. [7]

2.3.3 Interparticle distance

The breaking of agglomerations results in smaller agglomerations that have shorter average distance between them. Hatzel et al. [2] report on the particles that are distributed more uniformly under high shear rate, increasing the electrical conductivity of the fluid. A more quantitatively relation between these factors will be described in section 2.3.4.

2.3.4 Conduction as a function of shear rate

Youssry et al. [16] provided a series of results from their rheo-electrical experiments. Their results show the effect of the shear rate $\dot{\gamma}$ on the apparent viscosity μ and the conductivity Σ (which will be denoted as σ in this report) of a fluid containing aqueous carbon black. A stress-controlled rheometer Physica MCR 101 (Anton Paar) was used to obtain these results. To obtain reproducible results, before each measurement the samples have been pre-sheared at a shear rate of $10^3 s^{-1}$ to remove mechanical history. After pre-shearing, the sample is left at rest before recording the data. Figure 13 displays the results of their experiments with one of the samples graphically. In this experiment, the volume fraction of carbon particles is $\phi_{CB} = 0.021$. In table 1, the values of their results can be found, obtained with the use of an online digitizer [11].

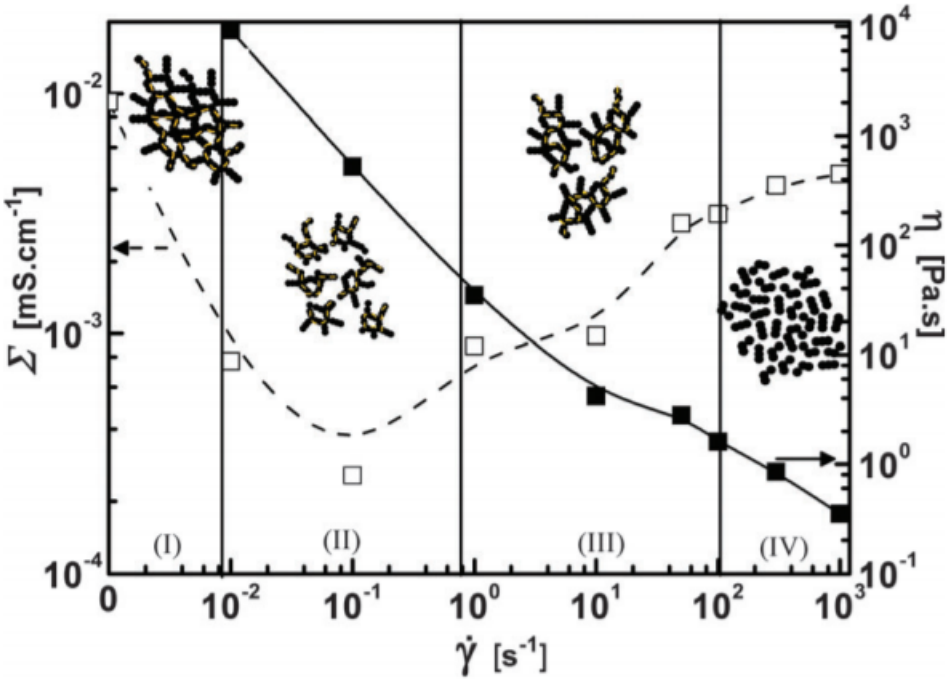

Figure 13: Conductivity Σ and apparent viscosity $\dot{\gamma}$ for different shear rates of a carbon black-based suspension with carbon concentration $\phi_{CB} = 0.021$ [16]. The open squares represent the measured conductivity; the filled squares the apparent viscosity, both at same values for shear rate.

Shear rate [s^{-1}]	Apparent viscosity [Pa s]	Conductivity * 10^{-3}[mS cm^{-1}]
0	17097*10	9.276
0.0101	9162.7	0.7686
0.1004	526.64	0.2559
1.005	36.055	0.8849
10.09	4.2945	0.9813
50.05	2.8556	2.865
99.00	1.6413	3.177
298.6	0.88995	4.134
1008	0.37121	4.671

Table 1: Results from rheo-electrical experiments provided by Youssry et al. [16]. Values extracted from graph of figure 13. The value for the apparent viscosity at $\dot{\gamma} = 0 s^{-1}$ is not measured, but has been obtained through extrapolation of a fitted function through the measured points.

Figure 13 shows a relation between the shear rate on one hand and the conductivity and apparent viscosity on the other hand. This figure does not represent a general relation for all fluids. To elaborate, figure 14 shows the results of Youssry et al.[16] for fluids with varying volume fractions ϕ_{CB} of carbon black.

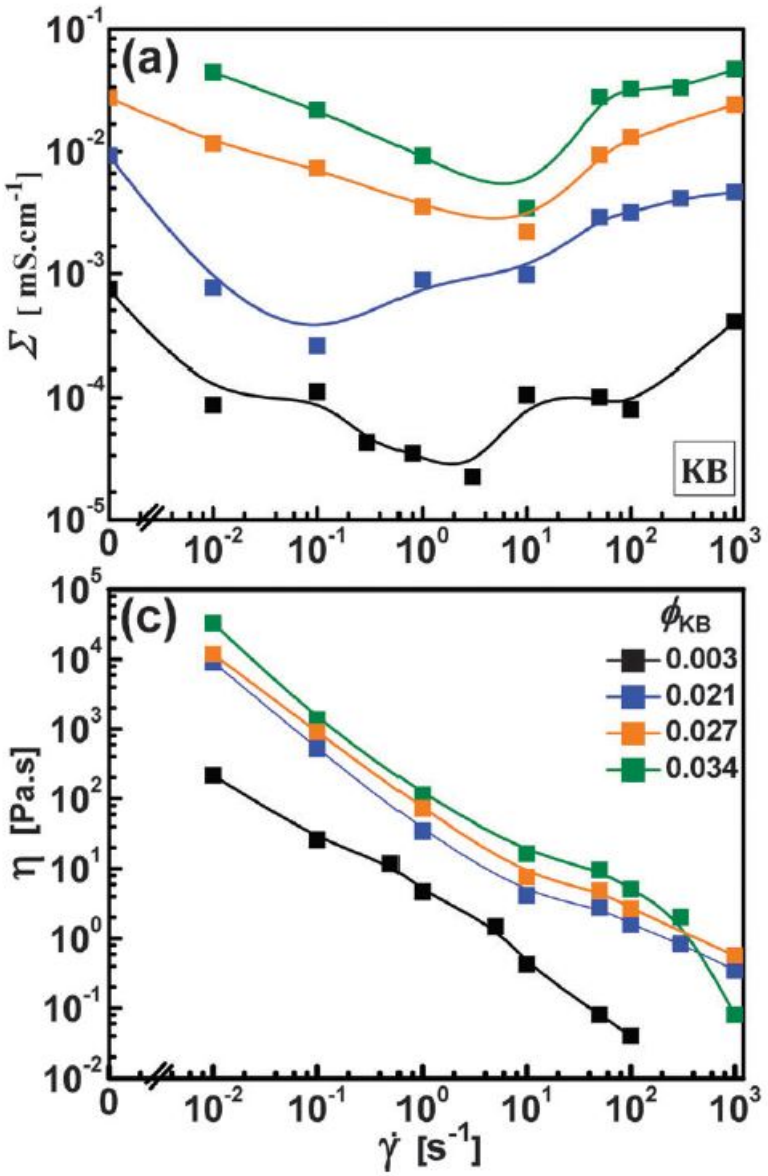

Figure 14: (a) Conductivity and (b) apparent viscosity vs shear rates of different carbon black volume fractions ϕ_{CB} [16]. The blue lines ($\phi_{CB} = 0.021$) represent the data from figure 13. The black (0.003), orange (0.027) and green (0.034) lines represent the data from the same measurements with fluids only varying the carbon black volume fraction ϕ_{CB}

3 Numerical setup for percolation

3.1 Percolation Theory

From the percolation theory, we see that the probability of network formation between two plates strongly depends on the concentration of conducting elements in a 3D system (see figure 9). When the percolation threshold is exceeded, the probability of the connection of two plates no longer depends on the distance between them. However, in the flow cell the power supply depends on the electrical conduction between the current collector and the active material. Every volume space has the same probability of containing active material. Therefore, for every point in the flow cell, a different percolating network is required to connect the active material to the current collector.

3.2 Programmed simulation

A MATLAB [8] script has been written to simulate the probability of network formation between a plate (the electrode) and a single point (active material). In this paragraph the simulation will be explained step by step. The script consists of two *functions* that both have an input and output. The input of these functions are the parameters that determine the output:

1. The first function requires 4 input values. Three for each dimension of the 3D system, n, m and o, and one for the probability p of an element representing a conducting particle. The output of this function is a three-dimensional array with uniformly distributed conducting elements and insulating elements. The function adds another type of elements to the array, called electrode elements. As in a real flow cell half the electrode covers one side of the system. Therefore, on top of the array, at $n = 1$, an electrode is placed with same width and length as the array. Figures 15 and 17 give a visual (2D) representation of an example of the output.

2. The second function requires only the array of the first function as an input. The function then determines for every element in the array that contains a conducting particle whether or not it has one side in common with the electrode. If it does, the conducting element changes into an "electrode element" as well. If not, the element stays a conducting element. The process is repeated until the electrode elements have no side in common with a conducting element anymore. Figures 16 and 18 show the examples of figures 15 and 17 after the output of function 1 has been used as an input of function 2.

The scripts for these functions are presented in appendix A. The output of the first function is determined randomly while the second function only has one possible output depending on the input.

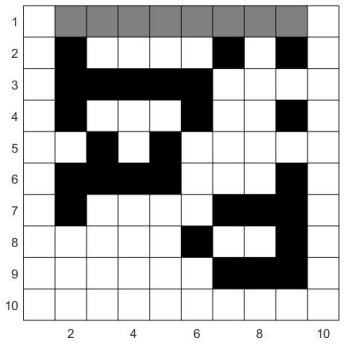

Figure 15: An example of a created array (in 2D) with $\phi = 0.40$. This is and output of function 1. The number of rows of the array is n, the number of columns is m or o, depending on which of the two horizontal dimensions is left out. The columns on the left and the right and the bottom row are left blank to function as electrically insulating material.

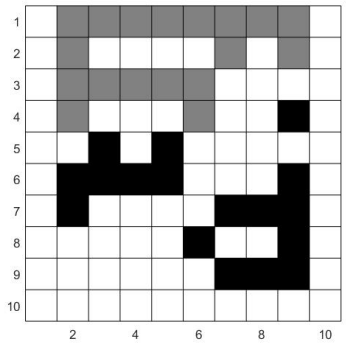

Figure 16: The created array with $\phi = 0.40$ as an output of function 2

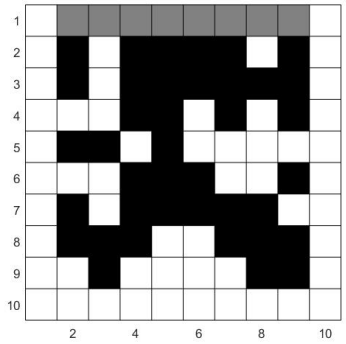

Figure 17: An example of a created array (in 2D) with $\phi = 0.60$. This is and output of function 1.

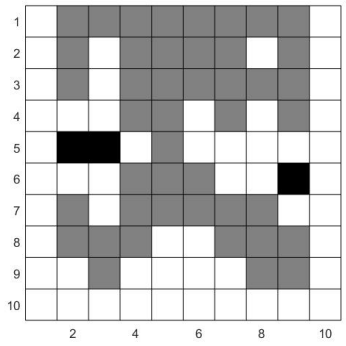

Figure 18: The created array with $\phi = 0.60$ as an output of function 2

Even though the figures representing an output of the first function are obtained randomly, the effect of change in the volume fraction of conducting particles on the fraction of "electrode elements" is clearly visible, as in figure 18 a larger fraction of the original conducting particles has become an electrode element than in figure 16. The fraction of conducting elements in the output of function 1 that have become electrode elements in the output of function 2 (the original electrode elements in row $n = 1$ excluded) is denoted as the spanning strength $\langle P \rangle$. The spanning probability between two random elements is the probability both of these elements have at least one side in common with the same cluster of conducting particles. Because the connection between an element and the electrode depends on whether or not the element has at least one side in common with an electrode element after function 2, the spanning probability between the electrode and a random element is equal to the probability of this element having at least one side in common with an electrode element.

4 Results

In this chapter the results of the simulation will be shown. Section 4.1 will present the results of the simulation of the percolation theory. In section 4.2 the data of table 1 will be used to derive a relation between the shear stress and the conductivity and the resistivity. Section 4.3 presents common flow profiles and combines the characteristics of these profiles to the relevant interpretation of the relations derived in section 4.2.

4.1 Percolation theory

4.1.1 Spanning probability $\langle \Pi \rangle$

As shown in figure 9a, the probability of two plates being connected, the spanning probability, depends on both the volume fraction of carbon particles and the height of the cell. In the flow cell however, active material can only exchange electrons when it is in contact with the electrode. To determine the spanning probability between a plate and an element with distance d to the plate, an array is made with the steps described in section 3.2. If a random element at height $n = d$ has at least one side in common with and "electrode element", this array is marked as a successful attempt. If the element at height $n = d$ has sides in common with only conducting elements or insulating elements, this array is marked as a failed attempt. Since the result of the process depends on the random placement of conducting particles, this is called a stochastic process and needs to be repeated to determine the spanning probability. After repeating this process 1000 times, the spanning probability becomes the fraction of successful attempts of the total number of attempts. The spanning probability is a stochastic function of the point-to-plate distance d and the volume fraction of conducting particles. Figure 19 shows the spanning probability as a function of the volume fraction of conducting particles for three different point-to-plate distances.

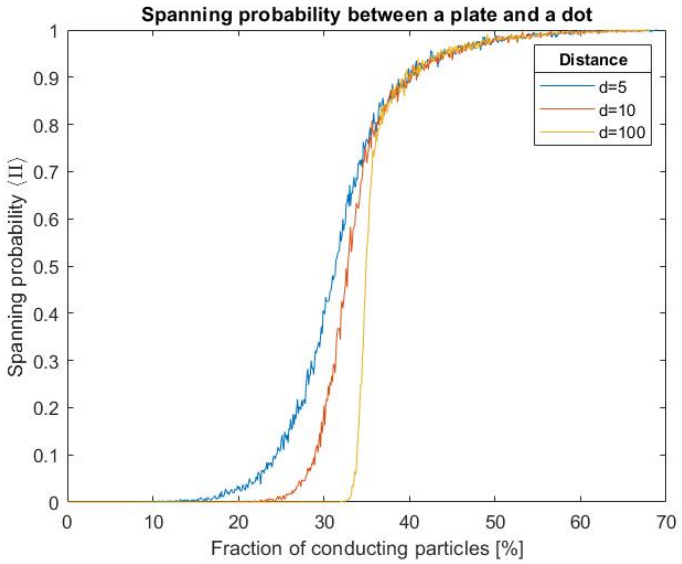

Figure 19: Average spanning probability vs volume fraction ϕ for three point-to-plate distances. The process is repeated 1000 times for each volume fraction.

With the variation of the point-to-plate distance, the graph in this figure clearly shows a lower spanning probability for larger distances in the volume fraction region of $20\% \leq \phi \leq 34\%$. This can be seen as an increase in the percolation threshold for larger distances. To achieve a spanning probability in the region of $0.2 \leq \langle \Pi \rangle \leq 0.5$, the required volume fraction strongly depends on the distance d. However, the curves for different point-to-plate distances collapse for high spanning probabilities in the region of $0.7 \leq \langle \Pi \rangle \leq 1.0$. The percolation threshold for this region is not affected by the distance d. This can be explained by zooming in on the location of the active material in the array. For the active material to be connected to the electrode it requires at least one neighbouring element to be a conducting element. Similarly, this conducting element needs to have a neighbouring conducting element as well, which it can connect with. And so fort, until the cluster of the active material is large enough to be connected to the cluster of "electrode elements". To give these clusters enough space to expand in all directions, the active material is placed at least 10 squares from the vertical and lower 'walls' of the array. The probability of the formation of a cluster containing the active material is

independent of array size. The electrode however, due to its size, has a much higher probability to be part of large extended clusters and is unlikely to be insulated if the active material is not. Therefore the bottleneck above the percolation threshold is the formation of a cluster containing the active element. To elaborate, figures 20 and 21 show a situation in which a large cluster containing the electrode has been formed. However, certain conducting elements can still be insulated. The 8th element of the 4th column is insulated, despite being surrounded by the electrode cluster, and is therefore an example of how a high fraction of conducting elements can still mark a failed attempt.

To summarize: even if a cluster extends to almost the entire system, the probability of a random element being left out of this cluster does not depend on the distance from the electrode. The bottleneck is the connection of the observed element to surrounding elements.

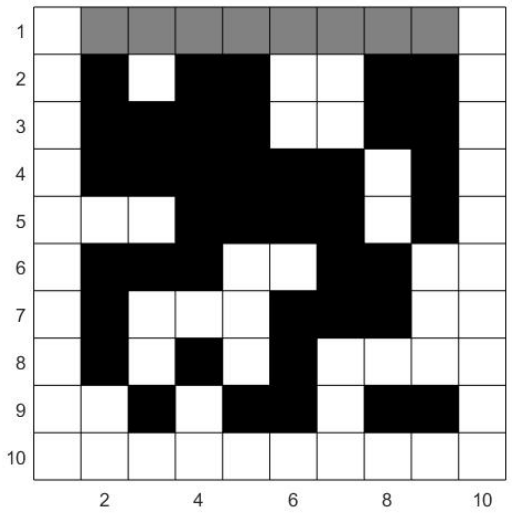

Figure 20: An example of a created array (in 2D) with $\phi = 0.60$. This is and output of function 1.

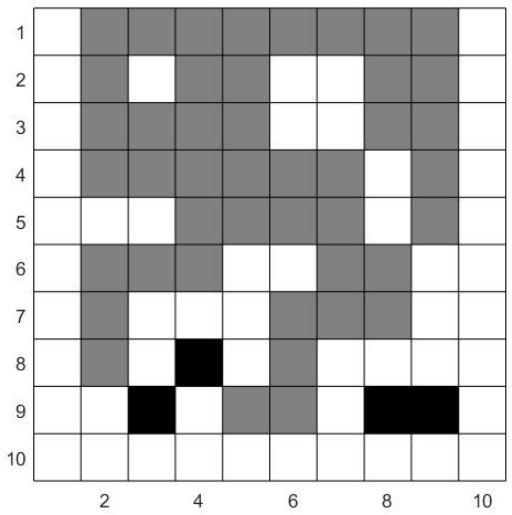

Figure 21: The created array with $\phi = 0.60$ as an output of function 2

4.1.2 Spanning strength $\langle P \rangle$

Every volume space has the same probability of containing active material. Therefore each element in the array contains an even amount of active material. Not only does the active material absorb or release electrons, it can transport electrons between different carbon black particles as well. As stated in section 2.2.2, the spanning

strength is the volume fraction of the medium that is connected to the plate. Just like the spanning probability, since the spanning strength of the array depends on the distribution of conducting and active material elements, the spanning strength is a stochastic function of the cell dimensions and volume fraction of carbon black and active material. In figure 22 the average spanning strength of arrays with a height of 100 and 1000 elements is compared. For each fraction of conducting elements, the average of the spanning strength of 100 randomly created arrays is calculated.

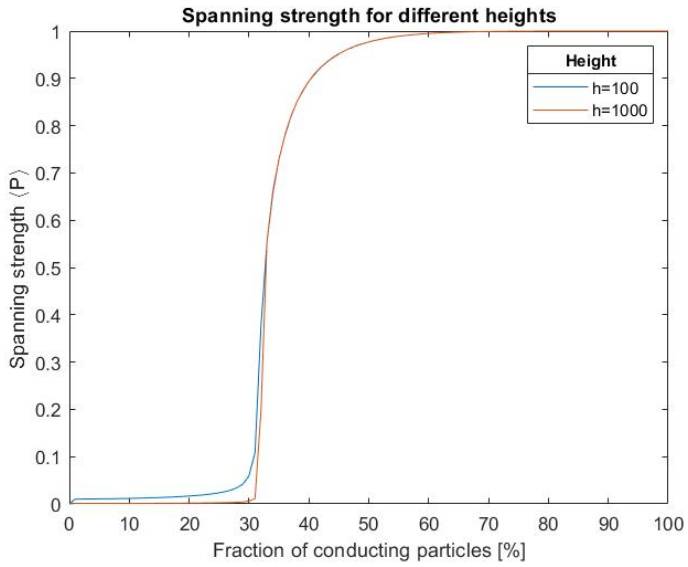

Figure 22: Average spanning strength for arrays with a height of 100 and 1000. The width in both directions is 100 elements.

In figure 22, it is clearly visible that the percolation threshold for high values of the spanning strength does not depend on the height of the cell significantly. The only spanning strengths for which the two curves can be clearly distinguished are in the region of $0 \leq P \leq 0.1$. This significant difference between both curves for low spanning strength can be explained by zooming in on the upper row of the array, below the electrode. In this row all of the black squares will, after applying function 2 to the array, become grey squares because of their connection to the original electrode elements. For low volume fractions of conducting elements, black squares in the remaining $h-1$ rows have a low probability of becoming grey squares. Therefore the spanning strength for low volume fractions is estimated by the fraction of black squares in the upper row N_1 divided by the total amount of black squares N_{tot}. By average, the fraction of black squares in the upper row divided by the total amount of black squares is equal to the inverse of the cell height $\frac{N_1}{N_{tot}} = \frac{\frac{N_{tot}}{h}}{N_{tot}} = \frac{1}{h}$. The spanning strength for low fractions of conducting elements When the carbon percentage, the fraction of black squares, approaches the percolation threshold, the grey squares start to reach more rows until eventually the curve converges at the percolation threshold of roughly $\phi = 0.33$.

To summarize, this first row is by definition connected to the electrode. This is why $\langle P \rangle$ for small h is significantly larger than 0.

4.2 Application of extracted data

From the values for shear rate and apparent viscosity (see table 1), the shear stress can be determined using equation 2. Since we also have a relation between the shear rate and the conductivity, a relation can be derived between the shear stress τ and the conductivity σ. Figure 23 shows this relation, along with a fitted curve obtained with the *cftool* function in MATLAB. This fitted curve is a rational function with second grade polynomials in the numerator and the denominator. The obtained equation 3 represents the conductivity (in $mS * cm^{-1}$) as a function of the shear stress:

$$\sigma(\tau) = \frac{0.00633 * \tau^2 - 0.6758 * \tau + 19.17}{\tau^2 - 15.28 * \tau + 1863} \tag{3}$$

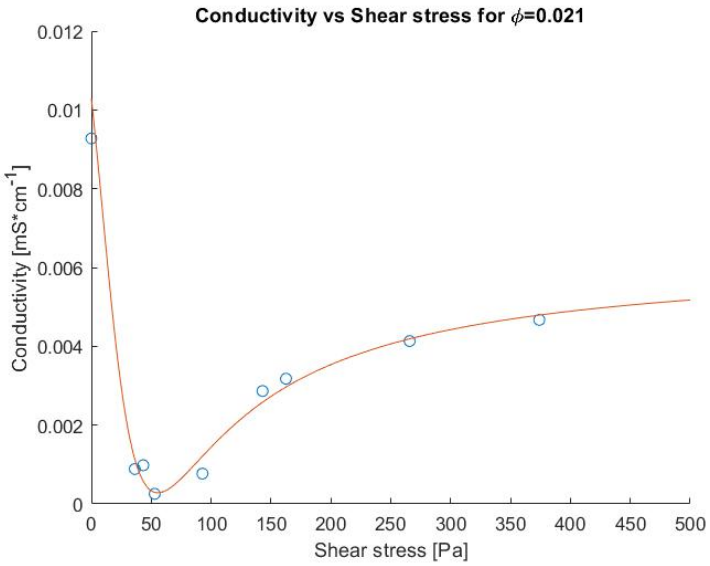

Figure 23: Variation of conductivity for different values of shear stress, calculated from data provided by Youssry et al.[16] The curve of equation 3 is fitted to the points.

To calculate the resistance over the entire cross-section of the flow cell, the local shear stress-dependent values for resistivity are required. The resistivity $[k\Omega * cm]$ is the inverse of the conductivity (equation 4).

$$\rho = \frac{1}{\sigma} = \frac{\tau^2 - 15.28 * \tau + 1863}{0.00633 * \tau^2 - 0.6758 * \tau + 19.17} \tag{4}$$

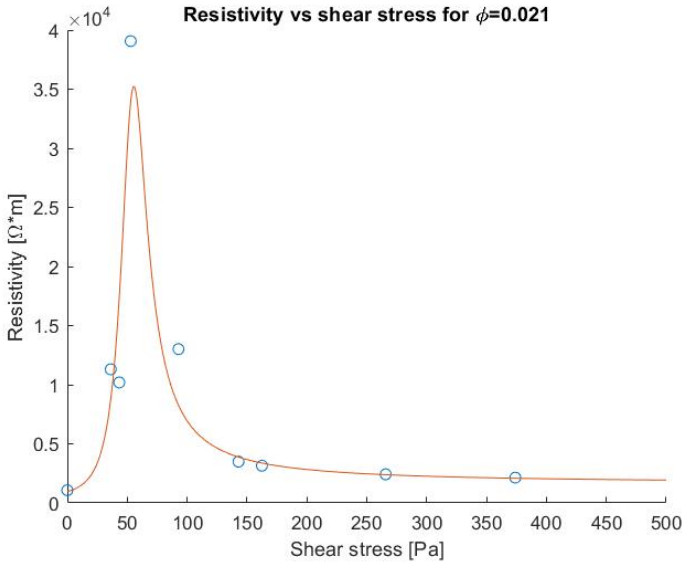

Figure 24: Resistivity as a function of shear stress

The total electrical resistance (in Ohm) of the fluid between the two electrodes, two infinitely large plates located at $x = \pm\frac{1}{2}H$, is the integral of the resistivity over the distance between the electrodes:

$$R = \int_{-\frac{1}{2}H}^{\frac{1}{2}H} \frac{\rho(x)}{A(x)} dx \tag{5}$$

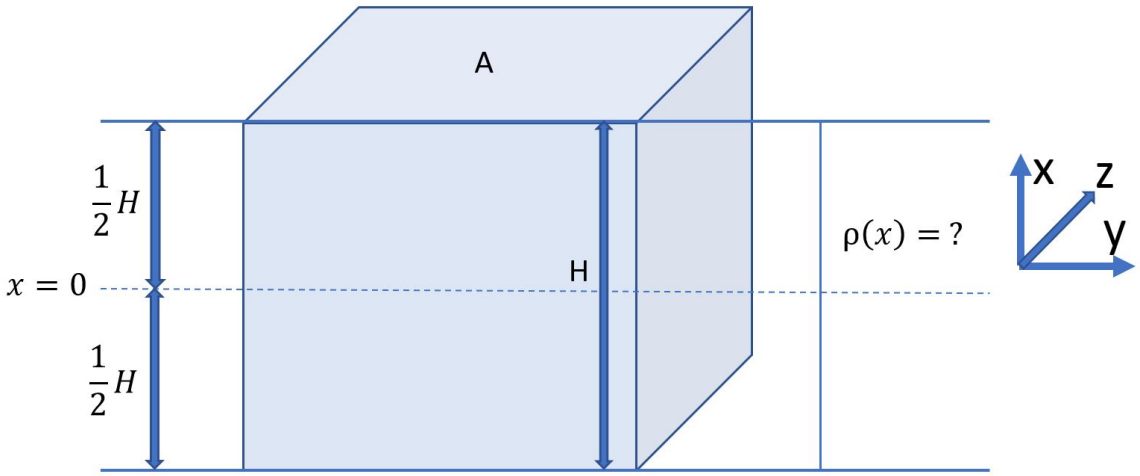

Figure 25: Schematic representation of the electrically conducting system between two electrodes. The profile of $\rho(x)$ depends on the type of flow (see section 4.3).

Here $\rho(x)$ is the resistivity of a slice at position x. The position $x = 0$ is the center of the flow. Since the flow is assumed to be developed and in steady state, all variables are independent of y, being the flow direction. A(x) $[m^2]$ is the surface area of an imaginary slice of the medium, perpendicular to the electric current, at height x and can be assumed constant through x. As a result, the electrical resistance per electrode surface area R*A $[\Omega m^2]$ is:

$$R * A = \int_{-\frac{1}{2}H}^{\frac{1}{2}H} \rho(x)dx \tag{6}$$

The conductivity and resistivity depend on the absolute value of the local shear stress, assumed that the flow profile is in steady state and the mechanical history of each point of the flow profile is representative for the experiments performed by Youssry et al. In section 4.3 the shear stress profiles in the most common flow systems are presented.

4.3 The electrical resistance in various laminar flows

In this paragraph the assumption will be made that all flows are in steady state and that the flow is created in the same way as Youssry et al. carried out their experiments [16] [7].

4.3.1 Couette flow

In a Couette flow, the fluid between two parallel plates flows as a result of the relative parallel movement $\vec{v_c}$ of one of the plates with respect to the other. Initially, due to the shear stress, the fluid at the surface of the moving plate starts moving in the same direction. After a while, when the fluid flow is in steady-state, the shear stress is constant over the distance between the two plates. In figure 26, the constant for shear stress τ_c is a result of the tangential motion of the upper plate, which moves in the y-direction with velocity v_c. To determine the conduction of the suspension in a Couette flow, the conductivity profile of the suspension is required. As a result of the invariant value for shear stress τ_c in a steady-state Couette flow cell, the conductivity (and resistivity) of the suspension is constant over the distance between the plates. This means that when the plate movement causes a shear stress at which the conductivity of the suspension is minimal, the conduction in the Couette flow cell is minimal. A quick look at the fitted curve of figure 23 tells us that this minimum is found around $\tau = 55Pa$. Using equation 3, we find a minimum at $\tau = 55.53Pa$. At this minimum, the conductivity of the suspension with carbon black volume fraction $\phi_{CB} = 0.021$ is $\sigma = 0.2835 * 10^{-3} mS * cm^{-1}$. Since the resistivity and conductivity of a Couette flow do not depend on the location x, equation 6 reduces to $R * A = \rho * l = \frac{1}{\sigma} * H$. For a Couette flow with height $H = 0.5cm$ the electrical resistance per electrode surface area is $R * A = 35.3 * 10^3 * 0.005 = 176\Omega * m^2$.

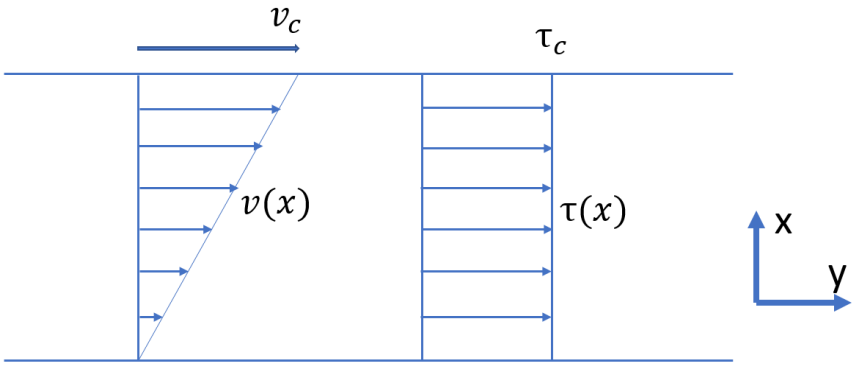

Figure 26: Velocity v and shear stress τ profile of a Couette flow

4.3.2 Poiseuille flow between two plates

A poiseuille flow is a flow caused by a pressure difference at both ends of a pipe or a body force such as the gravitational force $\overrightarrow{g}$. As with all gasses and liquids, the suspension flows in the opposite direction of the pressure gradient $\frac{dP}{dy}$. Just like in the case of the Couette flow, the shear stress is result of the fluid moving with respect to the walls. However, in this case the shear stress is not constant over the flow profile; around the central line between the two plates, the shear stress of a steady-state flow is anti-symmetric and linear. At this central line, the shear stress is zero. In figure 27, the shear stress and flow profile describe a Poiseuille flow.

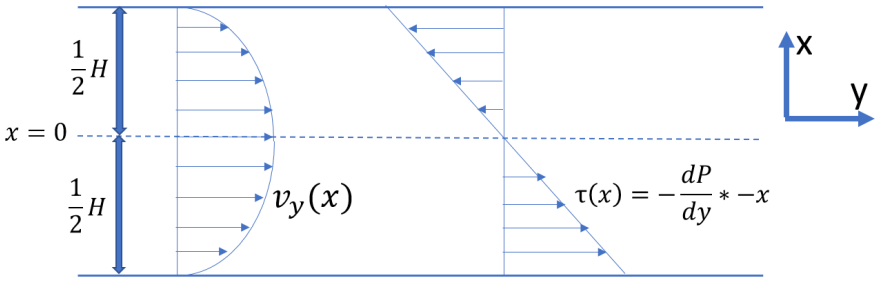

Figure 27: Velocity v_y and shear stress τ profile of a Poiseuille flow

As described in paragraph 4.2, the value of the resistivity depends on the absolute value of the shear stress. After taking the absolute value of the shear stress, the shear stress profile of the pure Poiseuille flow becomes symmetric with value $\tau = \tau_0 = 0$ in the middle between the plates. Since the shear stress profile of figure 27 describes a straight line, the absolute value for the shear stress grows proportionally with the deviation from the middle. The local value of the absolute shear stress [Pa] is calculated[14] with equation 7:

$$|\tau(x)| = -\frac{dP}{dy}|x| \tag{7}$$

Here, $\frac{dP}{dy}$ is the pressure gradient in the flow direction. As the fluid flow in this direction is positive, the pressure gradient is negative. With the relation between the absolute shear stress and x, values for the local conductivity at certain values $|x|$ can be determined by substituting equation 7 in equation 3. Now the conductivity at $\tau = 0$ represents the conductivity in the middle of the flow cell and the conductivity at $\tau = -\frac{dP}{dx} * \frac{1}{2}H$ represents the conductivity at the electrodes. Due to the linear relation between the deviation and the shear stress, where $\tau(0) = 0$ and the absolute shear stress grows proportionally with the deviation, figure 23 becomes the conductivity profile of one half of the Poiseuille flow cell and figure 24 becomes the resistivity profile.

To evaluate equation 6, since the absolute shear stress only depends on the absolute value of x, $\rho(x)$ is symmetric along the x-axis and the integral becomes:

$$R * A = 2\int_0^{\frac{1}{2}H} \rho(x)dx \tag{8}$$

To use equation 4, the argument of $\rho(x)$ needs to be replaced by τ. Using equation 7, the interval of integration becomes $0 \leq \tau \leq -\frac{dP}{dy} * \frac{1}{2}H$ and dx is replaced by $d\tau$. This leads to the integral:

$$R * A = \frac{2}{-\frac{dP}{dy}} \int_0^{-\frac{dP}{dy} * \frac{1}{2}H} \rho(\tau) d\tau = \frac{H}{-\frac{dP}{dy} * \frac{1}{2}H} \int_0^{-\frac{dP}{dy} * \frac{1}{2}H} \rho(\tau) d\tau \tag{9}$$

Here $-\frac{dP}{dy}$ can be determined by dividing the total pressure difference ΔP in the flow cell by the total length of the cell L, i.e. $-\frac{dP}{dy} = -\frac{P_2 - P_1}{y_2 - y_1} = -\frac{\Delta P}{L}$

Interesting in the Poiseuille flow cell is to look for a certain value of the pressure gradient at which the resistance per electrode surface area is largest. This upper value denotes the situation in which a Poiseuille flow cell would operate with the lowest power.

In equation 9 the term on the right side can be substituted by the term $\rho_{avg} * H$, where ρ_{avg} is the average resistivity in the Poiseuille flow. Here we see that the average resistivity only depends on the shear stress at the electrodes $\tau = -\frac{dP}{dy} * \frac{1}{2}H$. To calculate the resistance per electrode surface area only the knowledge of the height H and the pressure gradient $\frac{dP}{dy}$ of the flow are left to be determined. Figure 28 shows a graph of the average resistivity between $\tau = 0$ and the value for the shear stress at the electrodes. The shear stress at the electrodes equals the upper limit of the integral 9. The maximum average resistivity is found at $\tau = -\frac{dP}{dy} * \frac{1}{2}H = 77.6Pa$ and equals $\rho_{avg} = 1.383 * 10^4 \Omega * m$. An increase or decrease in the pressure gradient would therefore improve the efficiency of the battery. The pressure gradient of a Poiseuille flow with height $H = 0.5cm$ is $\frac{dP}{dy} = -\frac{\tau}{\frac{1}{2}H} = -\frac{7.6}{0.0025} = -31 * 10^3 Pa * m^{-1}$ at this maximum.

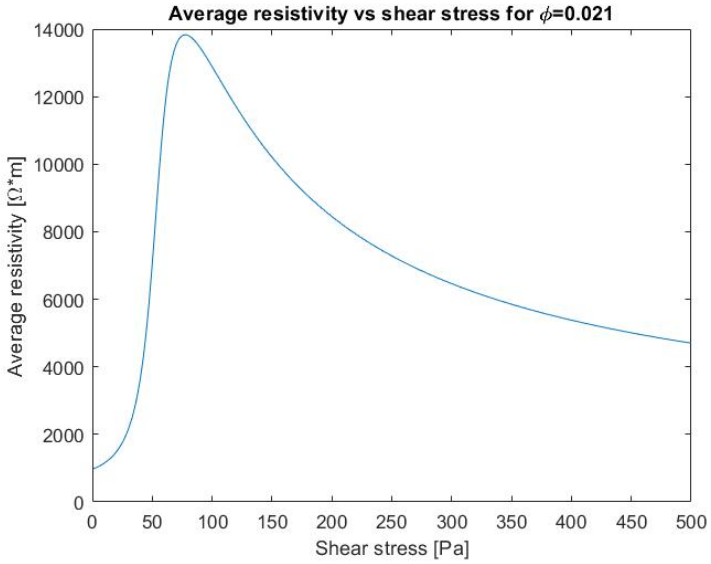

Figure 28: Average resistivity for different values for the shear stress at the electrodes

4.3.3 Velocity in the Poiseuille flow

When a pressure gradient is applied, the absolute value for the shear stress depends on the absolute value of the deviation from the centre of a Poiseuille flow cell, as displayed in figure **??**. For the one dimensional situation in section 4.3.2, the shear rate $\frac{dv_y}{dx}$ is the local derivative in the x-direction of the velocity v_y in the y-direction. From table 1 a relation can be derived between the shear rate $\dot{\gamma}[s^{-1}]$ and the shear stress, thereby using equation 2. The points in figure 29 are the result of this derivation.

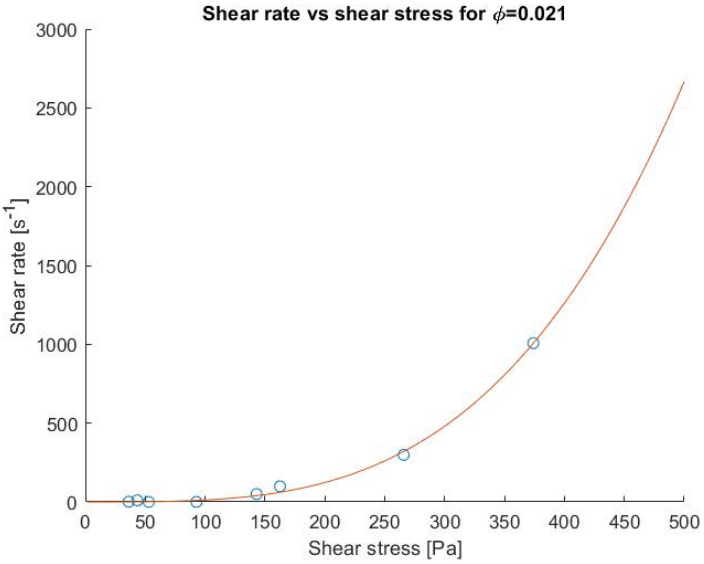

Figure 29: Variation for shear rate $\dot{\gamma}$ for different values for the shear stress τ along with the fitted curve, calculated from data provided by Youssry et al.[16]

The cftool function of MATLAB [8] earlier described is used to find values for a and b that fit a function of the form:

$$\dot{\gamma}(x) = a * (\tau(x))^b = a * \left(-\frac{dP}{dy}x\right)^b \tag{10}$$

For the specific fluid with $\phi = 0.021$, with MATLAB the constants a and b are found to be $a = 2.335 * 10^{-6}$ and $b = 3.356$. The fitted curve is found in figure 29 as well. From this equation and the fact that the velocity is zero at the walls ($x = \pm\frac{1}{2}H$), the velocity (in m/s) on position x can be calculated with:

$$v_y(x) = \frac{a}{b+1}(-\frac{dP}{dy})^b((\frac{1}{2}H)^{b+1} - x^{b+1}) \tag{11}$$

Note that only the upper half ($x \in \left[0, \frac{1}{2}H\right]$) is considered in equation 11 to ensure a positive base in x^{b+1}. The average velocity for a Poiseuille flow with height H can be calculated with:

$$v_{avg}(0 \leq x \leq \frac{1}{2}H) = \frac{1}{\frac{1}{2}H}\int_0^{\frac{1}{2}H} v_y(x)dx = a(-\frac{dP}{dy})^b\frac{1}{\frac{1}{2}H}\left(\frac{(\frac{1}{2}H)^{b+2}}{b+1} - \frac{(\frac{1}{2}H)^{b+2}}{(b+1)(b+2)}\right) = \frac{a}{(b+2)}(-\frac{dP}{dy})^b(\frac{1}{2}H)^{b+1} \tag{12}$$

In this representation, the pressure gradient is a constant and the average velocity depends only on the height of the cell. However, since $\tau_{max} = -\frac{dP}{dy}\frac{1}{2}H$ we can substitute for $\frac{1}{2}H$ and formulate equation 12 again:

$$v_{avg}(0 \leq \tau \leq \tau_{max}) = \frac{a}{(b+2)}(\frac{\tau_{max}}{\frac{1}{2}H})^b(\frac{1}{2}H)^{b+1} = \frac{a}{(b+2)}(\frac{1}{2}H) * (\tau_{max})^b \tag{13}$$

With this relation, the graph of figure 28 can be redrawn with values for the average velocity on the x-axis to get the relation between the average velocity and the average resistivity in the flow cell. Below, figures can be found showing a graph of the relation between the average velocity and the average resistivity. Since the average veolcity depends on the height of the cell, as can be seen in equation 13, this height is taken constant in each of the graphs.

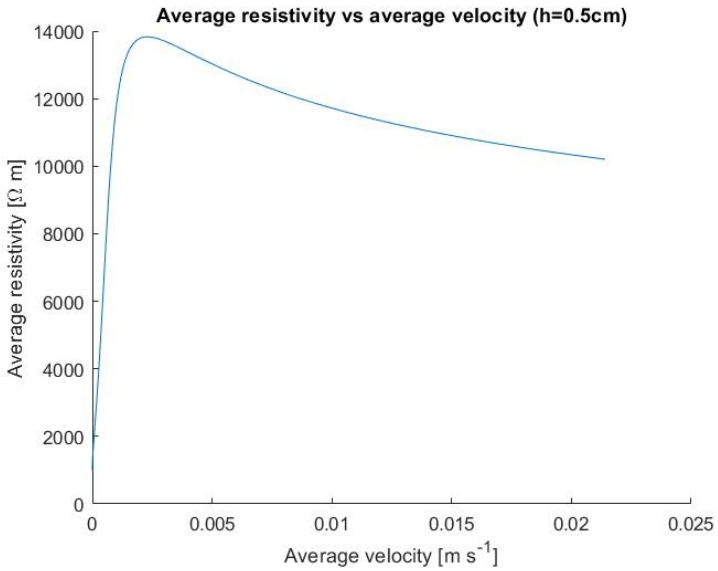

Figure 30: Average resistivity vs the average velocity in a Poiseuille flow with a height of 0.5 cm

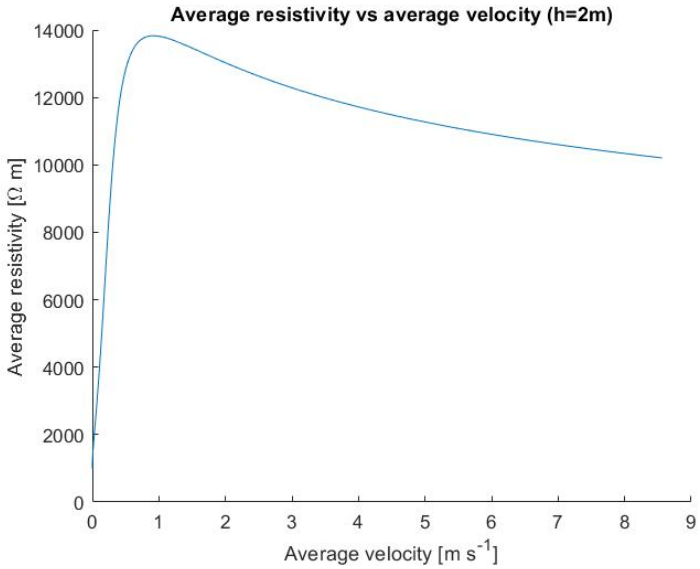

Figure 31: Average resistivity vs the average velocity in a Poiseuille flow with a height of 2 m

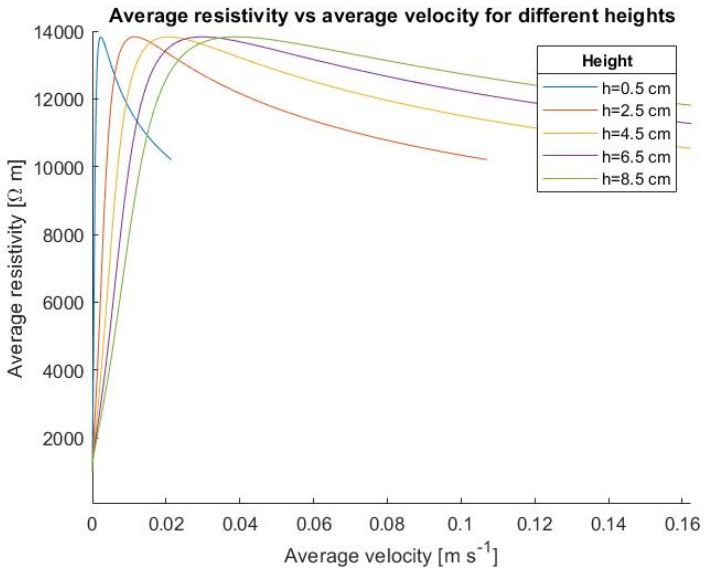

Figure 32: Average resistivity vs the average velocity in a Poiseuille flow with different heights

For each of the graphs of figures 30, 31 and 32, the maximum of the average resistivity has the same value. This value is also found in figure 28. This peak however, is found at different values for the average velocity in each of the graphs. When the Poiseuille flow has a height of 0.5 centimeter this peak is found at a velocity of 2.87 millimeter per second, whereas this peak is found at a velocity of 1.15 meter per second in a Poiseuille flow with a height of 2 meters. From symmetry of the absolute shear stress profile around the x-axis, we know that the average resistivity between the two walls of the flow is equal to the average resistivity between the active material and one wall of the flow, provided that the active material in a steady-state flow is uniformly distributed over the x-axis.

4.3.4 Poiseuille flow in the flow cell

The situation of section 4.3.2 does not fully represent a flow cell, as most flow cells have comparable height and width. The discussed Poiseuille flows however are assumed to be of infinitely large width so the profile can be simplified to a 2D problem. In this section the relations between the shear stress and the conductivity and resistivity of equations 3 and 3 are applied to a Poiseuille flow between four walls. The flow profile of an incompressible Newtonian fluid[5] is given by:

$$\vec{v} = v_y * \vec{j} = v_{max} * \left(1 - \left(\frac{x}{L_x}\right)^2\right) * \left(1 - \left(\frac{z}{L_z}\right)^2\right) \tag{14}$$

The shear stress components can be calculated with equation 2 and therefore are:

$$\tau_{yx} = \mu * \left(\frac{dv_y}{dx}\right) = -\mu * v_{max} * \left(1 - \left(\frac{z}{L_z}\right)^2\right) * \left(\frac{2x}{L_x^2}\right) \tag{15}$$

$$\tau_{yz} = \mu * \left(\frac{dv_y}{dz}\right) = -\mu * v_{max} * \left(1 - \left(\frac{x}{L_x}\right)^2\right) * \left(\frac{2z}{L_z^2}\right) \tag{16}$$

Note that in these equations the viscosity is a constant over the flow profile, which defines a Newtonian fluid, and the apparent viscosity in the previous sections is not. Therefore the situation of this section does not fully represent the flow cell of a SSFB either. However, this section gives an indication of the shear stress and conductivity and resistivity profiles if the steady-state Poiseuille flow is created with the same mechanical history as the experiments of Youssry et al.[16] and shows the effect of changes in these profiles. In figures 33 and 34 respectively the x-component τ_{yx} and the z-component τ_{yz} of the shear stress are expressed in terms of the maximum shear stress at the wall τ_{max}, which, if $L_x = H = W = L_z$, is equal to:

$$\tau_{max} = (\tau_{yx})_{max} = \frac{2 * \mu * v_{max}}{L_x} = \frac{2 * \mu * v_{max}}{L_z} = (\tau_{yz})_{max} \tag{17}$$

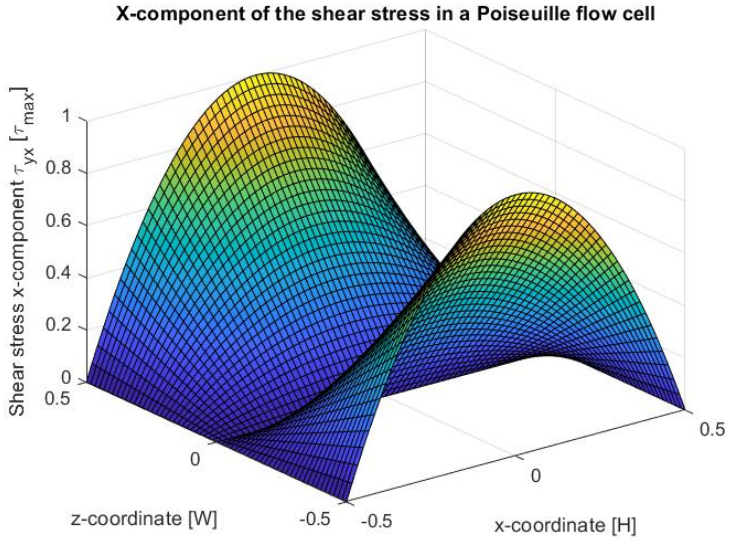

Figure 33: X-component of the shear stress in a Poiseuille flow cell

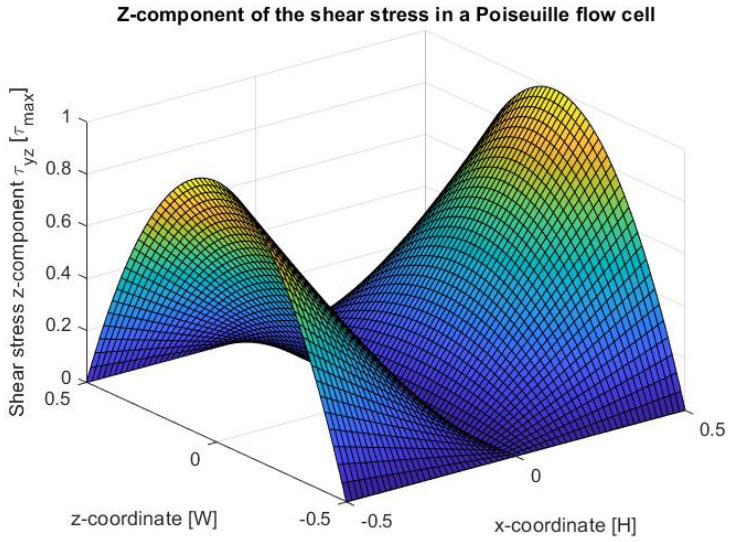

Figure 34: Z-component of the shear stress in a Poiseuille flow cell

The absolute value of the shear stress now is calculated with:

$$|\tau| = \sqrt{\tau_{yx}^2 + \tau_{yz}^2} \tag{18}$$

The figures 33 and 34 can be combined to one 3D-plot of the absolute shear stress. For the case where $H = W$, figure 35 displays this plot.

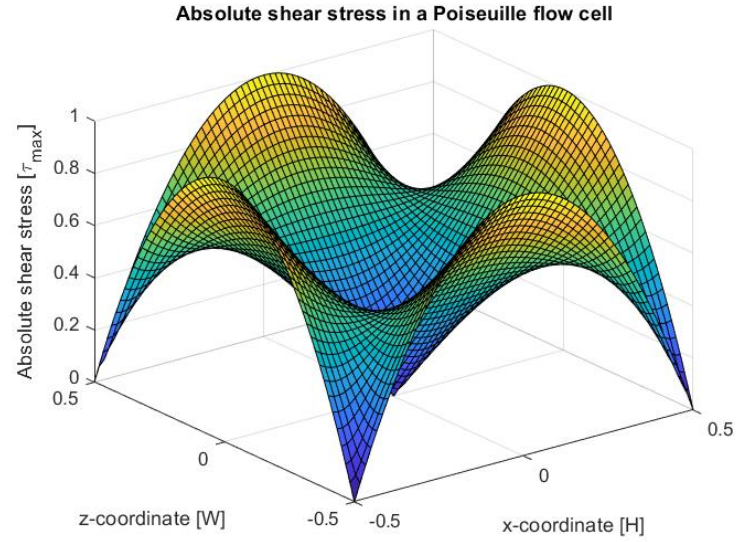

Figure 35: Absolute shear stress profile in a Poiseuille flow cell

With equations 3 and 4 the conductivity and resistivity profiles can be calculated as well (figure 36 and 37)

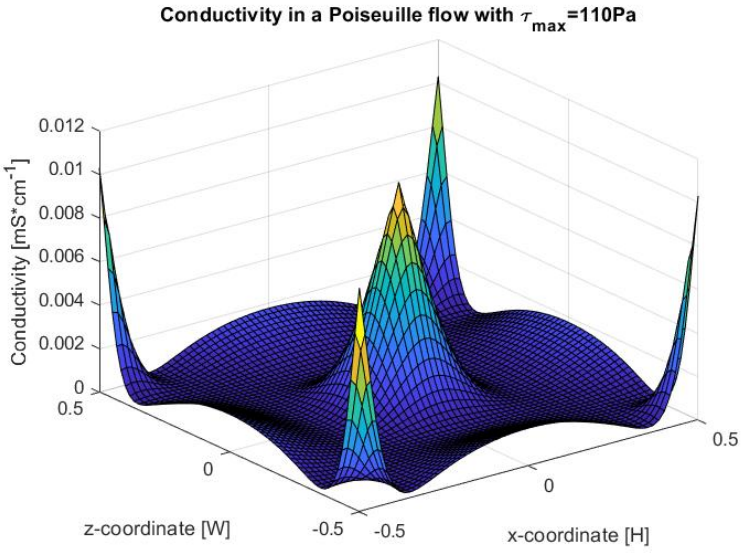

Figure 36: Conductivity profile in a Poiseuille flow cell

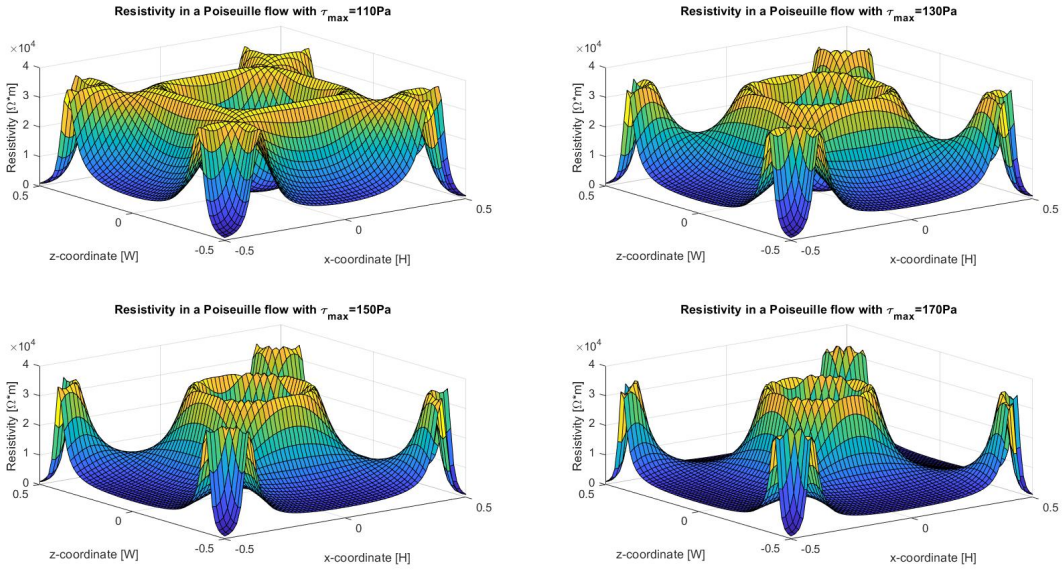

Figure 37: Resistivity profile in a Poiseuille flow cell for different values for τ_{max}

In figure 37, 4 different resistivity profiles are displayed, all of which describe the absolute shear stress profile of figure 35, with one difference: τ_{max}. The increase of the maximum shear stress at the walls generates different resistivity (and conductivity) profiles.

Note that in a flow cell only two opposite sides of the fluid are covered by the electrodes. Calculation of the resistance from a certain point inside this flow cell to an electrode gets more complicated, as the electrons do not just follow a straight path to the electrode. Electrons follow all paths available in inverse proportion to the impedance (resistance) of the paths[3]. According to the principle of *The path of least resistance*, the largest fraction of electrons follow a path through the system where the integral of the resistivity curve is lowest.

Even though calculation of the exact electrical resistance between an electrode at $x = -\frac{1}{2}H$ and an electrode at $x = \frac{1}{2}H$ is complex, in the resistivity profiles of figure 37 one clear observation can be made: a significant change in the average resistivity of the paths of least resistance. Since electrons in the Poiseuille flow with $\tau_{max} = 170Pa$ do not follow paths with 'mountains' (the yellow values) of high resistivity like the electrons in the Poiseuille flow with $\tau_{max} = 110Pa$, the expected conductivity between electrodes in these Poiseuille flows strongly varies. If a steady-state Poiseuille flow is established with the same steps as in the experiments carried out by Youssry et al.[16], an increase of the maximum absolute shear stress can have positive effects on the electrical conductivity.

5 Discussion

With results often comes uncertainty. This uncertainty can have a variety of causes. In this chapter the uncertainty of results from different methods of this report will be presented

5.1 Obtaining data from graphs

The data from the figure 13 has been obtained by digitization of the figure in an online digitizer. Although extraction of data with this method is done manually, the website provides high precision. Uncertainties following this procedure can therefore be neglected.

5.2 Fitting the curve

Using the *cftool* function of MATLAB, it is possible to fit a function to a given set of points. However, used method works best if as many points as possible contribute to a function with as few as possible function parameters. The used dataset provided 9 points and the relation between shear stress on one hand and conductivity and shear rate on the other hand can be better determined when the experiment of Youssry et al. [16] is repeated for more known values of the shear rate.

Equation 3 came out as the best fit to the given dataset for $\phi = 0.021$ consisting of values for the conductivity σ and their corresponding values for the shear stress τ. This function is a rational function with second order polynomials in both the numerator and the denominator, in the form of equation 19.

$$f(x) = \frac{p_1 * x^2 + p_2 * x + p_3}{x^2 + q_1 * x + q_2} \tag{19}$$

Here p_1, p_2, p_3, q_1 and q_2 are constants calculated with the use of MATLAB. This method also gives a 95% confidence interval for each of these values. The 95% confidence intervals for these values are $0.002716 \leq p_1 \leq 0.009944$, $-1.149 \leq p_2 \leq -0.2028$, $0.9509 \leq p_3 \leq 37.39$, $-166 \leq q_1 \leq 135.5$ and $61.22 \leq q_2 \leq 3665$. As can be seen in figure 23, the fit matches the data well. However, the 95% confidence interval will be smaller if more points are used to fit a function to. Smaller 95% confidence intervals indicate a more accurate relation between the conductivity and the shear stress. Figure 38 displays the dataset and the curve of figure 23, along with the 95% confidence interval of the curve. As we can see, The 95% confidence interval has boundaries which are shaped almost identically to the fitted curve. Therefore, only the exact conductivity in the fluid can differ slightly from the measured values of the experiments carried out by Youssry et al. [16]. The values for shear stress at which a peak in the (average) resistivity is found will not differ much from the calculated ones.

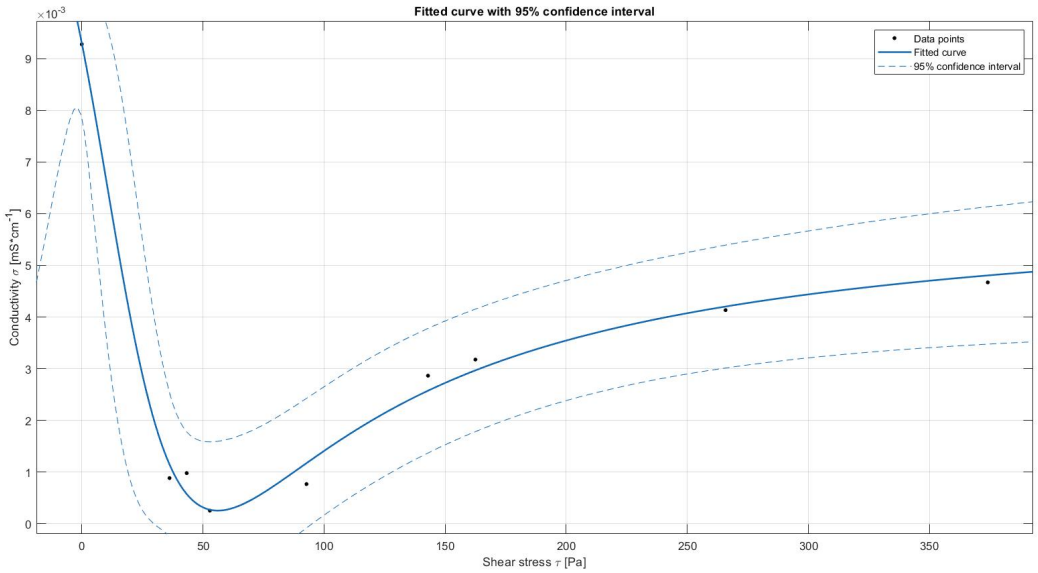

Figure 38: 95% confidence interval along with the fitted curve of the relation between the conductivity and the shear rate

Equation 13 gives the relation between the average velocity in a Poiseuille flow with $\tau_{max} = -\frac{dP}{dy}\frac{1}{2}H$ the shear stress at the walls. However, a and b in this equation are constants calculated with the use of matlab as well. The confidence intervals for these values are $2.9 * 10^{-6} \leq a \leq 7.57 * 10^{-6}$ and $2.975 \leq b \leq 3.736$. Figure 39 displays the dataset and the curve of figure 29 along with the 95% confidence interval of the curve. Obviously, changing the values of a and b does not change the values for the conductivity or the shear stress in of the figures in this report. However, since equation 13 is used to substitute the values of the average shear stress with values of the average velocity, the value for the average velocity corresponding to each value for the average resistivity changes upon changing a or b.

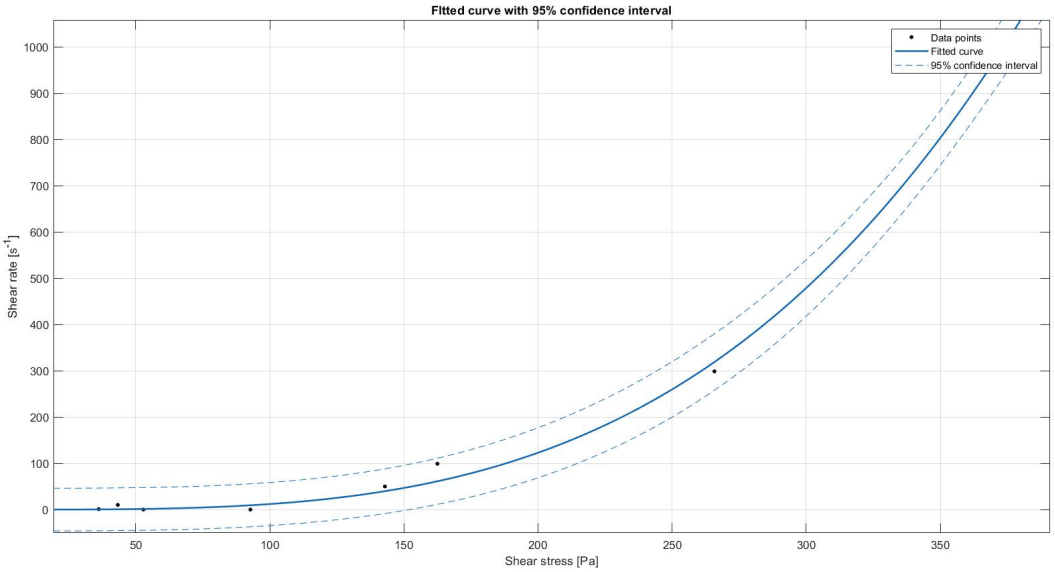

Figure 39: 95% confidence interval along with the fitted curve of the relation between the shear rate and the shear stress

6 Conclusions

The research question was: How does the electrical conduction relate to the height and width of the flow cell, the carbon black concentration in the fluid and the flow profile of the fluid? The effects of these parameters have been investigated from two different perspectives: by simulating the percolation theory and by analyzing the rheo-electrical properties of the fluid in the cell.

6.1 The effect of cell height

From the perspective of the percolation theory, the height of the cell does not affect the spanning strength of the system. Only for flow cells with unrealistically small dimensions, which for example less than a million particles would fit in, the height of the cell affects the possibility of bridge formation and the percolation threshold.

From equation 9, we know that the height of the cell is related to the electrical conduction, since the resistance of the cell is proportional to the distance electrons have to travel inside a system with invariant average resistivity.

Since the spanning probability (figure 19) and spanning strength (22) in systems with a high carbon black volume fraction ($\phi \geq 35\%$) does not depend on the height of the cell, this is in contrast to the relation in equation 9. Therefore, these results can not be combined to a single function.

6.2 The effect of cell width

For the width of the cell the same principle holds according to the percolation theory: when the percolation threshold is reached, large clusters of conducting particles can be formed. These clusters inevitably span an entire system, independent of the width of the cell.

Again from equation 9, we know that the width of the cell is related to the electrical conduction, since the electrical resistance of the cell is inversely proportional to the width of the cell. This relation only holds under the assumption that the surface of the electrodes increases proportionally to the width of the cell.

6.3 The effect of carbon black concentration

When the percolation threshold is exceeded, large clusters of conducting particles are formed. Increasing the carbon black volume fraction will not have large influence on the formation of these clusters. On the other hand, if the carbon black volume fraction is too low to create large clusters, a decrease will not yield significant effect either.

From figure 14, we know that different volume fractions of carbon black cause different conductivity measurements. From this figure it is clear that an addition to the volume fraction increases the conductivity of the fluid.

Both experiment show an increase in the (possibility of) electrical conductivity for higher volume fractions of carbon black or conducting materials. However, the conductivity changes more slowly in the experiments of Youssry et al.[16] than the spanning strength and spanning probability did in the simulation of the percolation theory.

6.4 The effect of the flow profile

As described in section 2.2.2, the percolation theory does not say anything about the effect of the flow profile on the electrical conduction.

The figures in sections 4.3.1 and 4.3.2 describe a relation between the shear stress and the average electrical resistivity in respectively the Couette flow cell and the Poiseuille flow cell. Both curves in the graph of these figures show a peak at a certain shear stress. In section 4.3.3 the relation between cell height, pressure gradient and velocity has been taken in account, resulting in a relation between the average velocity and the average resistivity in a 2D Poiseuille flow

7 Recommendations

7.1 General relation

The results of chapter 4 show a clear effect of different factors on the conduction in a Semi-Solid Flow Battery. These effects are significant enough to take in account when assembling the flow cell for a SSFB. During this project, the main goal was to find the relation between the flow profile and the electrical conduction in the flow cell, due to the fact that little is known about this relation. The graphs of figures 30, 31 and 31 show a clear relation between the average velocity in flow cells and the average resistivity. However, this relation is derived for a specific composition of materials in a fluid. Even though the experiments of Youssry et al. have been repeated for different volume fractions of carbon black, the results do not give insight in the effect of shear rate on apparent viscosity and conductivity of all fluids containing aqueous carbon black. For fluids with different compositions, new measurements are required to determine the optimal parameters such as the carbon black volume fraction, the height of the cell and the applied pressure gradient.

7.2 Smaller 95% confidence intervals

Furthermore, this relation is based on the dataset of table 1. As described in section 5.2, this dataset only consists of 8 à 9 points and the fitted curve relies on 5 coefficients. As a consequence, these coefficients have large 95% confidence intervals. This leads to high uncertainty when calculating for example the critical shear rate or average velocity at which the (average) resistivity reaches its peak and starts decreasing. To narrow down these 95% confidence intervals, the experiments of Youssry et al. should be repeated for a higher density of values for the shear rate.

7.3 Obtaining realistic data

Finally, the balance between shear stress and colloidal forces is not reached instantaneously and depends on the mechanical history of the fluid, as section 2.3.4 describes. The process of agglomeration takes time and the mechanical history of the fluid is decisive for the formation of agglomerations. In the SSFB, the mechanical history does not include a period in which the fluid is pre-sheared, since this would cause energy loss due to friction. By varying the shear rate in the experiment between realistic values for the SSFB, the history of the fluid comes closer to the real situation. In this situation, the fluid experiences low shear rates for a long time (depending on the time spent in the reservoirs), and higher and variable short term shear rates (during the period in which it flows through the tubes and the flow cell).

References

Gallier, S., Lemaire, E., Peters, F., and Lobry, L. (2015). Percolation in suspensions and de gennes conjectures. *Physical Review*.

Hatzell, K. B., Boota, M., and Gogotsi, Y. (2015). Materials for suspension (semi-solid) electrodes for energy and water technologies. *Royal Society of Chemistry*.

Holt, M. (2001). The path of least resistance.

Ke, X. (2018). Fundamental studies on transport phenomena in redox flow batteries with flow field structures and slurry or semi-solid electrodes: modeling and experimental approaches.

Kundu, B., Simlandi, S., and Das, P. K. (2011). Analytical techniques for analysis of fully developed laminar flow through rectangular channels. *Research Gate*.

LLC, W. (2020). Percolation threshold.

Ma, F., Fu, Y., Battaglia, V., and Prasher, R. (2019). Microrheological modeling of lithium ion battery anode slurry. *Journal of Power Sources*.

MathWorks (2018). Matlab r2018b.

Qi, Z. and Koenig Jr., G. M. (2017). Review article: Flow battery systems with solid electroactive materials. *Department of Chemical Engineering, University of Virginia,*.

Qi, Z., Liu, A. L., and Koenig Jr., G. M. (2017). Carbon-free solid dispersion licoo2 redox couple characterization and electrochemical evaluation for all solid dispersion redox flow batteries. *Elsevier*.

Rohatgi, A. (2019). Webplotdigitizer.

Smil, V. (2012). Energy transitions: History, requirements and prospects.

Solar, V. (2017). The seasons and solar energy.

Van den Akker, H. and Mudde, R. (2017). *Fysische Transportverschijnselen*. Delft Academic Press.

Weber, A. Z., Mench, M. M., Meyers, J. P., Ross, P. N., Gostick, J. T., and Liu, Q. (2011). Redox flow batteries: a review. *Journal of Applied Electrochemistry*.

Youssry, M., Madec, L., Soudan, P., Cerbelaud, M., Guyomard, D., and Lestriez, B. (2013). Non-aqueous carbon black suspensions for lithium-based redox flow batteries: rheology and simultaneous rheo-electrical behavior. *Royal Society of Chemistry*.

Appendices

Appendix A

```
1  function [A,geleid,grootte,random]=creatematrix(p,n,m,o) %3D matrix with 1s (
       conducting (p)) and 0s (insulating (1-p))
2      random=zeros(n,m,o);
3      A=zeros(n,m,o);
4      reductor=0;
5      oxidator=0;
6      grootte=(n-2)*(m-2)*(o-2);
7      geleid=0;
8      for j=2:m-1
9          for k=2:o-1
10             A(1,j,k)=-1;
11             for i=2:n-1
12                 random(i,j,k)=rand;
13                 if random(i,j,k)<p
14                     A(i,j,k)=1;
15                     geleid=geleid+1;
16                 end
17             end
18         end
19     end
20 end
```

```
function [perc_A,brug]=percolation(A,geleid)
    brug=0;
    nochange=0;
    perc_A=A;
    bla=round(0.25*(size(perc_A,1)-2)*(size(perc_A,2)-2)*(size(perc_A,3)-2)); % large enough to reach every element
    for s=1:bla
        if nochange==0 %stops when matrix remains unchanged
            nochange=1;
            for i=2:size(perc_A,1)-1
                for j=2:size(perc_A,2)-1
                    for k=2:size(perc_A,3)-1
                        if perc_A(i,j,k)==1
                            if perc_A(i-1,j,k)==-1
                                perc_A(i,j,k)=-1;
                                nochange=0;
                            end
                            if perc_A(i+1,j,k)==-1
                                perc_A(i,j,k)=-1;
                                nochange=0;
                            end
                            if perc_A(i,j-1,k)==-1
                                perc_A(i,j,k)=-1;
                                nochange=0;
                            end
                            if perc_A(i,j+1,k)==-1
                                perc_A(i,j,k)=-1;
                                nochange=0;
                            end
                            if perc_A(i,j,k-1)==-1
                                perc_A(i,j,k)=-1;
                                nochange=0;
                            end
                            if perc_A(i,j,k+1)==-1
                                perc_A(i,j,k)=-1;
                                nochange=0;
                            end
                            if perc_A(i,j,k)==-1
                                brug=brug+1;
                            end
                        end
                    end
                end
            end
        end
    end
end
```